Affinity hierarchies underlie the co-assembly of nucleolar and heterochromatin condensates in Drosophila embryos

Authors

Srivarsha Rajshekar[1], Omar Adame-Arana[2,3], Gaurav Bajpai[2], Kyle Lin[1], Serafin Colmenares[1], Samuel Safran[2], Gary H Karpen[1,4]

[1] Department of Molecular and Cell Biology, University of California Berkeley, Berkeley, USA

[2] Department of Chemical and Biological Physics, Weizmann Institute of Science, Rehovot, Israel

[3] Max Planck Institute for the Physics of Complex Systems, Dresden, Germany

[4] Division of Biological Sciences and the Environment, Lawrence Berkeley National Laboratory, Berkeley, USA

Correspondence: gkarpen@berkeley.edu

Abstract

Nucleoli are surrounded by Peri-Centromeric Heterochromatin (PCH), reflecting a close spatial association between the two largest biomolecular condensates in eukaryotic nuclei. We have investigated how this highly conserved organization is established *de novo* during early Drosophila development and whether these distinct condensates influence each other's 3D organization. High-resolution live imaging revealed a highly dynamic process in which the PCH progressively surrounds nucleoli through a series of stage-specific intermediates. To assess interplay between the condensates, nucleolus assembly was eliminated by deleting the ribosomal RNA genes (rDNA), resulting in increased PCH compaction and subsequent reorganization to a hollow shell. In addition, in embryos lacking rDNA, some nucleolar proteins were abnormally redistributed into new bodies or 'neocondensates,' including enrichment in the PCH hollow core. These observations, combined with computational modeling, led to the hypothesis that nucleolar-PCH associations are mediated by a hierarchy of affinities between PCH, nucleoli, and 'amphiphilic' protein(s) that interact with both nucleolar and PCH components. We identified the nucleolar protein Pitchoune as a candidate for such an amphiphilic protein because it also contains a PCH-interaction motif and fills the PCH hollow core in embryos lacking rDNA. Together, these results unveil a dynamic program for establishing nucleolar-PCH associations during animal development, demonstrate that nucleoli are required for normal PCH organization, and identify Pitchoune as a likely molecular link for stabilizing PCH-nucleolar associations. Finally, we propose that disrupting affinity hierarchies could cause cellular disease phenotypes by

liberating components that form 'neocondensates' or other abnormal structures through self-association and secondary affinities.

Introduction

The eukaryotic nucleus is organized into different membrane-less compartments known as biomolecular condensates that assemble via multivalent interactions between their constituent molecules. Prominent examples include the nucleolus, nuclear speckles, and heterochromatin, essential for cellular viability and function (Lyon et al., 2021; Shin & Brangwynne, 2017). An individual condensate can concentrate several distinct macromolecules in cells, including structured and intrinsically disordered proteins and nucleic acids. Condensates with the same components that nucleate at different cellular locations can coarsen or fuse into larger clusters, whereas condensates with distinct compositions do not fuse when juxtaposed (Ditlev et al., 2018). Nevertheless, in the crowded environment of the nucleus, distinct condensates coexist to display close, conserved associations to form higher-order complex structures (Fare et al., 2021). Although many studies have examined the formation and function of individual condensates, we know relatively little about the interplay between distinct interacting condensates *in vivo* with respect to how they form and impact each other's structure and function.

Two prominent nuclear condensates that are proximally located in a highly conserved manner are the Nucleolus and Peri-Centromeric Heterochromatin (PCH) (Bizhanova & Kaufman, 2021; Padeken & Heun, 2014). The nucleolus is a multi-layered biomolecular condensate that plays an essential role in the assembly of ribosomal subunits and forms by liquid-liquid phase separation of its constituent molecules (Brangwynne et al., 2011; Feric et al., 2016; Lafontaine et al., 2020). Nucleoli are localized to chromosome locations containing tandemly repeated ribosomal RNA genes (rDNA), and condensate formation is nucleated via the synthesis of ribosomal RNA (rRNA) by RNA-Polymerase I (RNA-Pol-I). Several proteins coordinate the processing of rRNA and its assembly into ribosomes before export from the nucleolus and nucleus (Pederson 2011). In most eukaryotic nuclei, the nucleolus is surrounded by PCH, a densely packed chromatin compartment that assembles on megabases of pericentromeric repeats, including tandemly repeated satellite DNA and transposable elements. While the nucleolus is the most transcriptionally active site in the nucleus, PCH is associated with transcriptional silencing and has essential roles in nuclear architecture and genome stability (Janssen et al., 2018). PCH is distinct from the inactive B compartment defined by Hi-C experiments since Hi-C analyses typically exclude the highly

repetitive PCH sequences (Lieberman-Aiden et al., 2009). Under the microscope, PCH can be visualized as dense chromatin regions enriched for the AT-rich DNA dye DAPI, histone modifications di- and tri-methylation of histone H3 (H3K9me2/3), and the cognate epigenetic reader Heterochromatin Protein 1 (HP1) (Politz et al., 2013). HP1 is a multivalent protein with structured and disordered domains (Eissenberg & Elgin, 2000) that undergoes phase separation *in vitro* and preferentially partitions DNA and nucleosomes (Keenen et al. 2020; Larson et al. 2017), while *in vivo,* it forms a liquid-like condensate nucleated by H3K9me2/3 enriched chromatin (Strom et al., 2017; Tortora et al., 2023; Wang et al., 2019).

A simple explanation for why PCH is organized close to the nucleolus is that tandem arrays of rDNA genes are positioned within pericentromeric satellite repeats on a subset of chromosomes (Potapova & Gerton, 2019). However, proximity mapping nucleolus-associated domains (NADs) and IF-FISH revealed that PCH sequences from chromosomes without any rDNA genes also associate with the nucleolus (Németh et al., 2010; Van Koningsbruggen et al., 2010). Thus, cis-proximity to rDNA is not necessary for PCH-nucleolar associations, and how PCH from all chromosomes becomes positioned around the nucleolus is unknown. Loss of the major nucleolar component nucleophosmin (NPM1) in human cell lines results in the reorganization of nucleolus-associated heterochromatin, suggesting a role for nucleolar proteins in PCH organization (Holmberg Olausson et al., 2014). Regardless, the proximal positioning of rDNA to PCH sequences is likely functionally relevant since not all rDNA genes are expressed, and a subset is silenced by heterochromatin formation (Srivastava et al., 2016). PCH repeats are dissociated from the nucleolus in senescent cells, suggesting that PCH-nucleolar association is linked to cellular health (Dillinger et al., 2017). Thus, the association of PCH and nucleoli is a prominent feature of 3D nuclear organization, with open questions about how the two condensates co-assemble and if they affect each other's structure and function.

This study uses early *Drosophila* embryos to simultaneously visualize the *de novo* co-assembly of PCH domains and the nucleolus. During the initial phases of formation, these two compartments are spatially separated and nucleate independently. After independent growth and fusions, the PCH is first associated with the nuclear edge, then progressively reorganizes around the nucleolus as the embryo develops. Mutational analyses that perturb heterochromatin disrupted nucleolar shape and morphology. Reciprocally, embryos that lack rDNA and, thus, a functional nucleolus show dramatic reorganization of PCH characterized by increased compaction followed by the formation of an abnormal hollow core. These results revealed that

nucleolar and PCH assembly, disassembly, and reassembly are highly dynamic during early development and identify an interdependency between the two nuclear condensates in their 3D organization. *In vivo* experiments and computational modeling showed that a hierarchy of interaction strengths between PCH, nucleoli, and 'amphiphilic' protein(s) able to interact with both nucleolar and PCH components could generate the layered organization of nucleoli and PCH. This hypothesis led to identifying Pitchoune, a DEAD-box RNA-Helicase protein, as a candidate molecular linker responsible for establishing or maintaining PCH-nucleolar associations. We discuss the potential impact of defective condensate associations and affinity hierarchies on abnormal phenotypes and disease states.

Results

PCH condensates and satellite repeats surround nucleoli in late Drosophila embryos

To define the 3D nuclear organization of established or 'mature' PCH and nucleolar condensates in Drosophila, we performed live imaging in late embryos (~12-16 hr, Embryonic Stage 14-16), larval tissues, and cultured S2 cells expressing fluorescently tagged transgenes for HP1a (Strom et al., 2017) and nucleolar proteins (Falahati & Wieschaus, 2017). Nucleoli are organized as di- or tri-layered liquid-like condensates; RNA Pol-I transcribes rDNA to form the innermost layer (Fibrillar Center or FC), rRNA is processed by proteins such as Fibrillarin to generate the Dense Fibrillar Compartment (DFC), and ribosomal proteins assemble with processed rRNA to form ribosomes in the outermost layer, the Granular Compartment (GC) (Feric et al., 2016; Thiry & Lafontaine, 2005). *Drosophila* nucleoli are also multi-layered as in other eukaryotes; the GC is marked by Modulo (the fly ortholog for Nucleolin), Fibrillarin marks the DFC, and Rpl-135, a subunit of RNA-Pol-I localizes within the Fibrillarin compartment (**Supplementary Figure 1A-B**).

We observed that the PCH condensate visualized using fluorescently tagged HP1a localizes around the nucleolus in late embryos, larval tissues, and S2 cells (**Figure 1A-B; Supplementary Figure 1C**), consistent with the 'canonical' organization conserved across eukaryotes. We used fluorescence *in situ* hybridization (FISH) combined with immunofluorescence (IF) to determine how PCH repeats from different Drosophila chromosomes (**Figure 1C**) are organized relative to the nucleolus. rDNA was enriched in two locations: high-intensity, compacted signals positioned just outside the nucleolus (likely representing silenced rDNA embedded within PCH) and weaker-intensity rDNA signals within the nucleolus (likely actively transcribing rDNA) (**Supplementary Figure 1D**). Consistent with their juxtaposition in cis on the X chromosome (**Figure 1C**), the long

359bp repeat array is located at the nucleolar edge (**Figure 1D)**. Notably, major pericentromeric satellite repeats (1.686) on autosomes that lack rDNA (Chr 2 and 3, **Figure 1C**) also localize to the nucleolar edge (**Figure 1D**). Irrespective of the linear distance from rDNA, the 3D distance of pericentromeric repeats 359bp and 1.686 to the nucleolar edge is comparable (**Figure 1E**). We conclude that PCH/HP1a surrounds nucleoli in late Drosophila embryos, and PCH DNA from chromosomes that do not contain rDNA also localizes to the nucleolar edge (**Figure 1F**). This is consistent with centromere clustering around nucleoli observed in various systems, including *Drosophila* cell lines (Padeken et al., 2013) and sequence mapping of Nucleolus-Associated Domains (NADs) in human and mouse cell lines that showed uniquely mapped heterochromatic sequences from all chromosomes contact the nucleolus (Bersaglieri et al., 2022; Van Koningsbruggen et al., 2010).

PCH-nucleolar associations change dynamically during early Drosophila embryogenesis

We next sought to visualize how PCH assembles around the nucleolus during initial condensate establishment, using high-resolution time-lapse imaging of early Drosophila embryos expressing RFP-Fib and GFP-HP1a transgenes. Drosophila embryos undergo 14 synchronized, syncytial nuclear divisions (S and M phases only) before cellularizing at blastoderm (cycle 14) and thereafter undergoing cell divisions (Farrell & O'Farrell 2014). Major chromatin features, including H3K9 methylation, are progressively established during the syncytial cycles (Ahmad & Henikoff, 2022; Seller et al., 2019). PCH condensates first emerge in cycle 11 interphase but have limited time for growth. In every subsequent cycle, they are dissolved in mitotic prophase and re-established in S phase (Strom et al., 2017). Nucleoli first emerge in cycle 13, seeded by transcribing rRNA (Falahati et al., 2016), dissolve in prophase, and re-form in subsequent interphases. Thus, cycle 13 is the earliest time PCH and nucleolar condensates appear in the same nuclei. Upon entry in cycle 13 interphase, HP1a and Fibrillarin proteins are initially diffuse throughout the nucleus, then within ~8 mins, each becomes enriched in multiple, distinct foci (**Figure 2A(i) and Supplementary Movie 1**). Small PCH and nucleolar condensates remain separated throughout cycle 13, likely because growth is limited by the short interphase (~15 mins) before dissolution in mitosis.

Cycle 14 begins like cycle 13 in that HP1a and Fibrillarin foci emerge soon after mitotic exit and are initially separated. However, PCH and nucleolar condensates grow larger and undergo liquid-like self-fusions or coarsening due to the extended length of cycle 14 interphase (~90 mins) (Falahati et al., 2016; Strom et al., 2017; Tortora et al., 2023) (**Figure 2A(ii) and Supplementary**

Movie 2). Notably, unlike the surrounded configuration observed in later embryo stages (**Figure 1**), by the end of cycle 14, only one small section of the HP1a domain is associated with Fibrillarin, corresponding to the rDNA locus on the sex chromosomes (**Supplementary Figure 2A-B**). The majority of the HP1a domain, including chromosomes 2 and 3, is distributed apically and juxtaposed to the nuclear periphery (**Figure 2A(ii) and Supplementary Figure 2C**). This 'extended' conformation represents a previously undescribed intermediate during the establishment of PCH-nucleolar associations (summarized in **Supplementary Figure 2D**).

Continued live and fixed imaging of HP1a and Fibrillarin in post-blastoderm, asynchronous cell divisions revealed how the extended PCH configuration dynamically transitions into the canonical surrounded form observed in later developmental stages (**Figure 2A(iii – v) and Supplementary Movies 3-5**). As in cycles 13 and 14, in each post-blastoderm interphase (cycle 15 onwards), HP1a and Fibrillarin proteins are initially diffuse, then nucleate into separate foci that grow and fuse to form the extended intermediate. The PCH remains in the extended configuration and predominantly associates with the nuclear periphery through the rest of cycle 15 (**Figure 2A(iii)**) but transitions between the extended and surrounded configurations during cycle 16 (**Figure 2A(iv)**). Finally, the first stable surrounded organization is observed ~15 min into cycle 17 interphase (**Figure 2A(v)**), after PCH condensates quickly transition through the extended configuration.

Complementary quantitative analyses substantiate these observed live dynamics of PCH and the nucleolus. First, the fraction of the nucleolar edge occupied by HP1a increases between cycles 14 and 17 (**Figure 2B**). Second, H3K9me2 displays the extended conformation relative to Fibrillarin in fixed Stage 8/cycle 15 embryos and localizes to the nucleolar edge later in development (**Supplementary Figure 3A)**. Third, immuno-FISH revealed that satellite repeats 1.686 on Chr 2 and 3 (**Figure 1C**) are located farther from the nucleolus in cycle 15 (Stage 8; mean=1.28μm) and display significantly more proximal localization in Stage 16 (mean=0.31μm) (**Figure 2C-D)**.

We conclude that PCH and nucleolar condensates first appear in cycle 13, but the canonical surrounded configuration is not stably established until cycle 17. Most importantly, PCH-nucleolar associations are highly dynamic during each interphase; both condensates undergo independent nucleation, growth, and fusions, then display cycle-specific spatiotemporal differences in

transitions between the extended (nuclear periphery) and surrounded (nucleolar periphery) configurations (summarized in **Figure 2A, schematic** and **Supplementary Figure 3B**).

Reduced levels of heterochromatin result in decondensed rDNA and enlarged nucleoli

Is the organization of PCH and nucleolar condensates interdependent? We investigated whether PCH is required for proper nucleolus formation by removing one of the major H3K9 methyltransferase genes Su(var)3-9. Su(var)3-9$^{06/17}$ embryos (Schotta et al., 2002) generated from Su(var)3-9$^{06/17}$ mothers are depleted for H3K9me2 in cycle 14 (**Supplementary Figure 4A**) and display a 1.5-fold increase in nucleolar volume compared to wild-type controls (**Supplementary Figure 4B-C).** In addition, combined immuno-FISH analysis revealed that the high-intensity rDNA block located at the nucleolar edge in wild-type was reduced in Su(var)3-9$^{06/17}$ embryos, with corresponding increases in the amount of dispersed rDNA within the nucleolus (**Supplementary Figure 4D**). Similarly, nucleolar size increased ~1.5 times in cycle 14 after maternal knockdown of HP1a using RNAi (**Supplementary Figure 4E-F**). We conclude that PCH restricts nucleolar volume and rDNA distribution (summarized in **Supplementary Figure 4G**). These results are consistent with previous studies showing HP1a/H3K9me2/3 enrichment at silent rDNA in flies and mammalian cells (Fefelova et al., 2022; Santoro et al., 2002). Further research is required to determine if the absence of H3K9me2/3 and HP1 alters nucleolar morphology by de-silencing rRNA transcription, versus a requirement for physical association with PCH condensates.

Embryos lacking nucleoli display abnormal PCH organization and neocondensate formation

Next, we determined if nucleolar condensates impact PCH organization by imaging RFP-HP1a and GFP-Fib in embryos that completely lack rDNA repeats (designated hereafter as -rDNA) due to the presence of a rearranged X chromosome (C(1)DX/0, Valencia et al., 1949). No functional nucleoli are formed in -rDNA embryos (Falahati et al., 2016), but they develop into late-stage embryos due to maternal deposition of ribosomes. Nucleolar proteins are redistributed to other nuclear locations in embryos lacking rDNA. For example, some (e.g., the GC component Modulo) become broadly dispersed in -rDNA nuclei (**Supplementary Figure 5A**). In contrast, while no nucleolus is present, the DFC component Fibrillarin forms spherical structures (as previously reported by Falahati et al. 2016) located at a significantly longer distance from the HP1a/PCH condensate compared to +rDNA controls (**Figure 3A-B;** +rDNA mean=1.78μm, -rDNA

mean=3.69μm, p<0.0001). These data suggest that Fibrillarin and HP1a proteins do not directly interact and thus do not mediate the canonical surrounded organization. Instead, we propose that Fibrillarin self-associations (Berry et al., 2015) and/or secondary affinities with other structures or molecules are sufficient to cause the formation of new, abnormal structures (hereafter termed 'neocondensates') when factors responsible for nucleolus nucleation (rDNA/rRNA) are not present.

Most importantly, PCH condensate morphology is significantly perturbed in embryos lacking rDNA. The "extended" HP1a conformation normally observed in cycles 14 and 15 is replaced by a more compact, rounded structure at the apical end of -rDNA nuclei (**Figure 3A, C**). The HP1a aspect ratio is significantly reduced compared to +rDNA controls (**Figure 3D;** +rDNA mean=1.96, -rDNA mean=1.40, p<0.0001), and pericentromeric repeats 1.686 (Chr 2 and 3) and AAGAG (all chromosomes) are more tightly clustered (**Figure 3E-F;** +rDNA mean=0.74μm, -rDNA mean-0.32μm, p<0.0001)).

Unexpectedly, in late-stage -rDNA Drosophila embryos, the PCH morphed from a hyper-compacted cluster to a hollow sphere-like structure, composed of HP1a surrounding a core devoid of HP1a (hereafter 'PCH void') (**Figure 4A-B**). To visualize this transformation at increased spatial resolution, we performed live imaging in the amnioserosa, whose large nuclei form a monolayer on the dorsal surface of the embryo during gastrulation (Lacy & Hutson, 2016). Live imaging of the amnioserosa nuclei in the developing -rDNA Drosophila embryo revealed the stepwise transformation of the compacted PCH to the formation of a progressively larger PCH void (**Figure 4C-D and Supplementary Movie 6**).

In addition to the absence of HP1a, the PCH void lacked the major nucleolar proteins Fibrillarin (**Figure 4A-B**) and Modulo (**Supplementary Figure 5A**), which formed neocondensates or were dispersed in the nuclear space (respectively), as observed in earlier -rDNA embryo stages. The PCH void did not contain DNA (DAPI staining), histones marked with H3K9me2 (IF), or any significant accumulation of RNAs (Propidium Iodide staining) (**Supplementary Figures 5B-D**). However, treatment with 488 NHS Ester, a pan-protein label (M'Saad & Bewersdorf 2020), revealed that the PCH void was enriched for unknown proteins (**Figure 4E**).

We conclude that PCH initially displays an atypical, hyper-compacted morphology in embryos lacking rDNA and nucleoli. Further, the PCH morphs into an abnormal donut-like structure whose

central core (the PCH void) lacks HP1a, nucleolar proteins, chromatin, and RNA but is filled with unknown protein(s) that may represent another neocondensate. Importantly, these results suggest that nucleoli are required for the normal distribution and organization of PCH condensates in nuclear space and provide insights into potential biophysical and molecular mechanisms responsible for PCH-nucleolar interactions.

Coarse-grained modeling predicts that amphiphilic proteins could mediate PCH-nucleolar organization in both +rDNA and -rDNA nuclei

Do unifying molecular interactions and biophysical parameters drive the dynamic establishment of nucleolar-PCH associations in wild-type embryos and PCH disorganization in the absence of rDNA? To address these questions, we used coarse-grained molecular dynamics simulations based on the following experimental observations and previous studies: 1) Fibrillarin and other nucleolar proteins have an intrinsic tendency to phase separate (Figure 3A) (Falahati et al., 2016; Feric et al., 2016), 2) PCH forms a condensate that associates with the nucleolus (Figure 1) (Strom et al., 2017), 3) there are no direct associations between PCH and Fibrillarin (Figure 3A), and 4) unknown proteins accumulate in the PCH void in -rDNA embryos (Figure 4E). We hypothesized that one or more proteins physically interact with both PCH and nucleolar components to generate the canonical 'surrounded' configuration in wild-type embryos. Due to their shared affinities for PCH and nucleolar components, we defined such proteins as 'amphiphilic' (etymology: Greek for 'likes both'). Such amphiphilic proteins have previously been described to regulate the structure of multiphasic condensates (Kelley et al., 2021). Further, we hypothesized that self-association/phase separation of such amphiphilic components would also form a protein-rich neocondensate that fills the PCH void in -rDNA mutant embryos.

To test our hypothesis, we modeled four minimal components (see details in Materials and Methods): (i) PCH (H) as a long, self-interacting polymer, (ii) rDNA (rD) as a polymeric block within the chromatin fiber that experiences good solvent conditions and is flanked by two PCH blocks, (iii) Fibrillarin (F) as a representative of a self-associating nucleolar protein, and (iv) an amphiphilic protein (X) that can phase-separate from the nucleoplasm and has binding affinities for both PCH and Fibrillarin/nucleoli (**Figure 5A**). Although Fibrillarin directly interacts with and processes transcribed rRNA (Berry et al. 2015; Falahati et al. 2016), we included an effective interaction between Fibrillarin and rDNA in the model to minimize the number of components. The theory of three-phase wetting of simple liquids demonstrates that a balance between the interfacial tensions of the different liquids determines the configuration of the phases involved (Torza & Mason, 1969).

Thus, we propose that to form the layered PCH-nucleolar organization, the self-associations of Fibrillarin must be stronger than those of the amphiphilic protein, which in turn must be stronger than the self-interactions of PCH since interfacial tension is proportional to the relative interaction strengths. These considerations led us to define a hierarchy of interaction strengths (rD-F=F-F>X-X>F-X>X-H>H-H) as a foundation for simulations using the parameters listed in the 4x4 interaction matrix, which recapitulated the canonical PCH-nucleolar organization observed *in vivo* (**Figure 5B and Supplementary Movie 7**). Further, PCH increases its association with the nucleolus when the concentration of the amphiphilic protein X is increased, predicting a mechanism for promoting PCH-nucleolar associations (**Supplementary Figure 6A-B**).

Various scenarios arise by changing the interaction strengths of the different components. For instance, reversing the hierarchy of self-interactions between protein X and Fibrillarin (i.e., X-X>F-F) leads to configurations in which complete wetting (surrounding) of the Fibrillarin-rich phase by the protein X-rich phase is not achieved (**Supplementary Figure 6C**). Increasing the attractions between PCH causes it to only partially wet the protein X phase (**Supplementary Figure 6D**). The detailed rationale for the choice of parameters and the range of affinities that recapitulate the *in vivo* configurations are described in the Methods section.

Setting the rDNA-Fibrillarin interactions to zero to model the consequences of eliminating the rDNA resulted in the formation of the protein X neocondensate within the PCH void and the spatially separated Fibrillarin neocondensate (**Figure 5C-D**). These phenotypes are observed in the simulations whenever the protein X – PCH interaction strength is greater than or equal to the X – Fibrillarin interactions (i.e., X-H≥F-X) (**Supplementary Figure 6E-F**). In the model, the nucleation of the new phase of amphiphilic protein X occurs within the PCH to reduce the cost of creating an interface of protein X facing the solvent. Instead, being surrounded by the PCH can reduce this interfacial energy, as expected from a wetting picture of simple liquids (Torza & Mason, 1969). In sum, simply eliminating the rDNA from this minimal model, and thus the ability to recruit nucleolar components such as Fibrillarin recapitulates both the PCH void filled with X protein and Fibrillarin neocondensate phenotypes observed in -rDNA nuclei *in vivo*.

We conclude that incorporating affinity hierarchies and an amphiphilic protein X into a minimal model recapitulates the observed *in vivo* organization of PCH and nucleolar condensates in both +rDNA and -rDNA conditions (**Figure 5B, C)**. Further, the experimental and simulation results indicate that the same amphiphilic protein(s) could mediate the surrounded configuration in wild-

type and accumulation in the PCH void in the -rDNA condition. This led us to predict that protein X should be a self-associating, outer nucleolar/granular compartment protein with an affinity for PCH components, such as HP1a.

The DEAD-box RNA Helicase Pitchoune, enriched at the interface between the nucleolus and PCH, forms a neocondensate within PCH in -rDNA embryos

The computational modeling results predicted that amphiphilic proteins interacting with both PCH and the nucleolus would be enriched in the PCH void in -rDNA embryos. Falahati & Wieschaus 2017 reported that the DEAD-Box RNA Helicase nucleolar component Pitchoune (Pit) (Zaffran et al., 1998) abnormally mislocalized in cycle 14 -rDNA embryos to the apical part of the nucleus, potentially co-localizing with the hyper-compacted PCH we observed in the absence of nucleoli (Figure 3A). Moreover, Pitchoune and its human ortholog DDX18 have an N-terminal disordered domain that could mediate self-association and/or nucleolar interactions, a helicase core, and a consensus PxVxL motif found in many HP1a binding partners (**Figure 6A**) (Thiru et al., 2004). To test the hypothesis that Pitchoune acts as the predicted amphiphilic protein X *in vivo*, we performed live imaging in Drosophila embryos expressing RFP-Fibrillarin and GFP-Pitchoune transgenes (Falahati & Wieschaus, 2017) in +rDNA and -rDNA genetic backgrounds. In +rDNA, Pitchoune localizes to the nucleolus with enrichment at the edge of Fibrillarin, suggesting that Pitchoune is enriched in the granular compartment, thus juxtaposed with the surrounding PCH (**Figure 6B**). However, in -rDNA embryos, Pitchoune and Fibrillarin do not associate and form separated, high-intensity spherical bodies (**Figure 6B**), suggesting that Pitchoune doesn't interact with Fibrillarin in the absence of rDNA and rRNA.

To investigate whether Pitchoune is enriched in the PCH void in -rDNA embryos, we performed live imaging in +rDNA and -rDNA embryos co-expressing Pit-GFP and RFP-HP1a transgenes. In cycle 14 +rDNA nuclei, Pitchoune localizes to the nucleolus while HP1a is in the extended form away from the nucleolus. In contrast, in -rDNA nuclei, a faint Pitchoune signal co-localizes with HP1a (**Figure 6C**). As the embryo develops, HP1a appears in the canonical form surrounding Pitchoune in +rDNA embryos. However, in -rDNA embryos, high-intensity Pitchoune puncta appear within each compacted HP1a condensate in cycle 17 epidermal nuclei and amnioserosa nuclei (**Figure 6C**). This revealed that the Pitchoune puncta/PCH void are first visible in cycle 17 in -rDNA embryos, the same developmental stage where the stable surrounded configuration is established in +rDNA embryos.

Time-lapse imaging of amnioserosa nuclei in -rDNA embryos revealed that the intensity of Pitchoune within HP1a is initially low and increases ~2.5-fold over an hour (**Figure 6D-E and Supplementary Movie 8**). Furthermore, the circularity of Pitchoune increases and approaches 1 (in projections) (**Figure 6F**), and the size of Pitchoune decreases over time (**Figure 6G**), suggesting that Pitchoune demixes from PCH to form a sphere, thereby minimizing its surface area due to its interfacial tension. Together, these data indicate that the nucleation and growth of Pitchoune within PCH creates a neocondensate whose emergence coincides with the formation of the PCH-void in -rDNA embryos. Notably, the predictions of the modeling results were validated *in vivo* and led to the discovery of Pitchoune as an example of a new class of amphiphilic proteins that interact with the nucleolus and PCH and likely stabilize the association between these condensates.

Discussion

This study presents four main findings about the organization of pericentromeric heterochromatin (PCH) and nucleolar condensates in the developing Drosophila embryo. Firstly, we observed that PCH-nucleolar associations are highly dynamic during initial establishment in early embryos, characterized by cycle-specific spatio-temporal differences in transitions between the extended (nuclear periphery) and surrounded (nucleolar periphery) configurations (Figures 1-2). Secondly, we have established a structural relationship between these two condensates, discovering that while PCH plays a role in restricting nucleolar size, the nucleolus facilitates the distribution of PCH components and repeats within the nuclear space (Figures 3-4). Thirdly, we have identified a hierarchy of interaction strengths between nucleolar and PCH components that contributes to their layered organization. Notably, the model predicted previously unrecognized protein(s) with 'amphiphilic' properties, which exhibit binding affinities to both the nucleolus and PCH (Figure 5). Lastly, we identified Pitchoune, a DEAD-box RNA-Helicase, as a potential candidate for such a novel amphiphilic protein (Figure 6). These findings provide insights into the co-assembly dynamics and organization of PCH and nucleolar condensates, contributing to our understanding of a prominent conserved feature of nuclear architecture.

Dynamics of PCH and nucleolar condensates

We discovered the process of *de novo* co-assembly of two prominent nuclear condensates, the nucleolus and PCH, at high spatial and temporal resolution in the naïve chromatin landscape of a developing Drosophila embryo. PCH and nucleolar condensates are nucleated independently and are initially spatially separated. As they grow and coarsen (self-fuse), one end of PCH is

tethered to the nucleolus via rDNA while the rest spreads along the nuclear edge to form an 'extended' intermediate before PCH from all chromosomes transitions to the canonical 'surrounded' configuration around the nucleolus. Lamina associations of uniquely mapped heterochromatin are well-characterized through the sequencing of lamina-associated domains (LADs) (van Steensel & Belmont, 2017). Recent studies mapping nucleolus-associated domains (NADs) demonstrated overlap between sequences associated with LADs and NADs (Bersaglieri et al., 2022; Bizhanova et al., 2020; Vertii et al., 2019). These studies reveal a relationship between the positioning of genomic loci to the nucleolar edge and the lamina, but mechanisms for these transitions remain unknown. Our study demonstrates a bulk reorganization of PCH from predominant association with the nuclear periphery/lamina to increased nucleolar contacts during cycles 14-17. We speculate that changes in chemical and/or biophysical properties facilitate the observed PCH-nucleolar dynamics. Potential contributing factors include reduced nuclear volumes, changes in relative volumes or material properties of nucleolar and PCH condensates, increasing H3K9me2/3 levels, or rRNA expression. Additionally, production or post-translational modifications of molecular factors (RNAs or proteins) like Pitchoune could alter binding affinities and stabilize PCH association with the nucleolus (discussed below).

Reciprocal regulation of PCH and nucleoli

The nucleolus is described as a nuclear hub that attracts heterochromatin (Padeken & Heun, 2014; Quinodoz et al., 2018). Our study expands on this knowledge by revealing that the nucleolus is required to properly distribute PCH condensates and repeats in nuclear space since, in the absence of the nucleolus, PCH self-attractions dominate to cause increased PCH compaction (Figure 3). Further studies are required to determine if the distribution of PCH around the nucleolus is functionally important, as the increased compaction could restrict critical nuclear processes like PCH transcription, repair, or replication. Reciprocally, genetic depletion experiments in the early Drosophila embryo revealed that the loss of H3K9me2/3 and HP1a causes rDNA decondensation and nucleolar enlargement (Supplementary Figure 4). This result could indicate that PCH condensates have a direct impact on nucleolar condensate structure and function. However, we favor the view that nucleolar enlargement reflects the role of heterochromatin in silencing the transcription of subsets of rDNA repeats and the partitioning of silent rDNA to nucleolus-associated heterochromatin (Németh & Längst, 2011; Pontvianne et al., 2013; Santoro et al., 2002; Van Koningsbruggen et al., 2010). This does not preclude the possibility that the surrounding PCH has independent roles in nucleolar functions, such as impact on ribosome export.

Together, we propose a model where PCH and nucleoli connected via a chromatin polymer (rDNA) regulate each other's spatial organization; the nucleolus distributes the PCH in the nucleus while the PCH constrains nucleolar size by limiting rDNA transcription and may impact other nucleolar functions. We predict that during aging and senescence, and perhaps other disease states, the balance of interactions between the PCH and nucleolus is perturbed to cause cellular phenotypes such as enlarged nucleoli (Buchwalter & Hetzer, 2017), decreased HP1a and heterochromatin (Larson et al., 2012), and the dissociation of PCH repeats from the nucleolus (Dillinger et al., 2017). While these cellular aging phenotypes are correlated, our model predicts a causative relationship between PCH and nucleolar changes, which remains to be tested.

Hierarchy of interactions underlies 3D structures of PCH and nucleolar condensates

Through computational modeling, we determined that a hierarchy of interaction strengths between a self-associating nucleolar protein (like Fibrillarin), PCH, and a self-associating linker protein that interacts with both the PCH and nucleolar condensates can recapitulate *in vivo* PCH-nucleolar organization in the presence and absence of rDNA (Figure 5). These predictions were validated by discovering that the DEAD-Box RNA Helicase Pitchoune associates with the outer nucleolar layer and PCH in +rDNA embryos and fills (and likely forms) the PCH void in -rDNA embryos (Figure 6). The multiphasic nature of the nucleolus was elegantly demonstrated, where sub-compartments form multiple immiscible phases within the nucleolus (Feric et al., 2016). The experiments in embryos lacking rDNA provide the insight that the different nucleolar phases can be decoupled by inhibiting pre-rRNA transcription, consistent with the hypothesis that layering results from 'vectorial transport' mediated by stepwise recruitment of phase-separating factors involved in rRNA transcription, processing, and ribosome assembly (Riback et al., 2020) (Figures 4 and 6). This study adds another layer to this organization to suggest some nucleolar components also stabilize physical associations with another condensate of distinct composition, the PCH. We propose that the association of the outer phase (granular compartment, GC) of the nucleolus with PCH is a consequence of a simple minimization of the interfacial energy of the GC components that associate with the PCH (defined in our study as 'amphiphilic components'). Further studies are needed to test the prediction that similar hierarchical associations are a general feature of higher-order multi-condensate structures.

DEAD-Box RNA Helicase Pitchoune: a novel player in stabilizing PCH-nucleolar interactions

This study identified the DEAD-Box RNA Helicase, Pitchoune, which typically localizes to the granular compartment of the nucleolus, as a self-associating molecule that interacts with PCH. Pitchoune is the fly ortholog of DDX18, which also localizes to the granular compartment (Zaffran

et al., 1998; Zhang et al., 2020). DDX18 associates with rRNA, and its yeast ortholog HAS1 is a ribosomal assembly factor (Dembowski et al., 2013; Zhang et al., 2020). We propose that Pitchoune can self-associate and phase separate (Falahati & Wieschaus, 2017) and interacts with HP1a since it consistently forms an abnormal spherical body (or neocondensate) within PCH in the absence of rDNA. We propose that Pitchoune associates with PCH to stabilize the PCH-nucleolus association via the conserved PXVXL domain in the C-terminus (Figure 6). Oligomerization of RNA-dependent DEAD-Box ATPases (DDXs) can promote the formation of RNA-rich condensates (Overwijn & Hondele, 2023). Curiously, Pitchoune neocondensates in –rDNA embryos first appeared in Cycle 17, coinciding with the cycle when the canonical "surrounded" conformation of PCH and nucleoli prominently appears in WT embryos. We hypothesize that an increase in Pitchoune concentration (beyond saturation) or affinity for HP1 (e.g., by post-translational modification) increases the cost of creating an interface with the nucleoplasm/solvent, thus promoting associations with PCH to minimize this interfacial energy. Several open questions remain regarding the mechanistic role of Pitchoune in PCH-nucleolar associations, which will be addressed in future studies.

Neocondensates in cellular pathology

Transcription of rRNA nucleates the assembly of nucleolar proteins into three distinct layers (Lafontaine et al., 2020). However, loss of the nucleating factor via deletion of rDNA in Drosophila embryos caused nucleolar proteins to display three distinct phenotypes; Modulo becomes broadly dispersed in the nuclear volume, while Fibrillarin formed a spherical body separated from the PCH, and Pitchoune fills or creates a void in the hyper-compacted PCH. These results highlight how disrupting condensate nucleation sites, or one set of interactions in a hierarchy of associations, can result in the formation of new, abnormal nuclear structures or 'neocondensates', due to inherent self-associations and/or secondary affinities of these factors with other structures or molecules. Since the cell contains several multi-component condensates, our results may have broader relevance since perturbing one set of interactions could give rise to new condensates/aggregates that cause defective cellular phenotypes or behaviors. Understanding these outcomes will also be relevant in cellular stress responses when new condensates are often formed, or the composition of existing condensates is perturbed (Alberti & Hyman, 2021).

MATERIALS AND METHODS

Key Resources Table

Reagent or Resource	Source	Identifier
Antibodies		
Rabbit anti-Fibrillarin	Abcam	ab5821
Mouse anti-H3K9me2	Abcam	ab8898
Mouse anti-Modulo	Gift from Mellone Lab (gift of Jacques Pradel, Chin-Chi Chen et al., 2012)	
Goat-anti-Mouse, Alexa Fluor 488	Invitrogen	A-11001
Goat-anti-Mouse, Alexa Fluor 568	Invitrogen	A-11004
Goat-anti-Rabbit, Alexa Fluor 488	Invitrogen	A-11034
Donkey-anti-Rabbit, Alexa Fluor 568	Invitrogen	A-10042
Bacterial Strains		
DH5α Competent Cells	This study	N/A
Chemicals		
DIG RNA Labeling Mix, 10x conc.	Roche	11277073910
DAPI	Sigma	D9542-10MG
Triton-X	Sigma	T8787
Commercial Bleach	Clorox	N/A
Formaldehyde Solution	Sigma	F8775
Halocarbon Oil 27	Sigma	H8773
Gas-permeable Lumox Film	Sarstedt	Catalog # 94.6077.317
Heptane	Sigma	246654
Methanol	VWR (EMD)	EM-MX0485-9
Bovine Serum Albumin	VWR	0332
VECTASHIELD® Antifade Mounting Medium	Vector Laboratories	H-1000-10
Atto 488 NHS Ester	Sigma	41698
Propidium Iodide Solution	Invitrogen	P3566
Critical Commercial Assays		
FISH Tag™ DNA Multicolor Kit,	Thermo Fisher	F32951

Alexa Fluor™ dye combination		
pGEM T-Easy Cloning Kit	Promega	A1360

Recombinant DNA

pGEM-rDNA	This study	N/A

FISH Probes

359bp	This study	N/A
1.686	This study	N/A
AAGAG	This study	N/A
rDNA	This study	N/A

Experimental Models and Subject Details

Fly Genotype	**Source**
Oregon-R	BDSC # 5
RFP-HP1a (2nd Chr)	Lipsick Lab (Wen et al., 2008)
GFP-HP1a (3rd Chr)	Lipsick Lab (Wen et al., 2008)
GFP-Fibrillarin	Weischaus Lab (Falahati and Wieschaus, 2017)
RFP-Fibrillarin	Weischaus Lab (Falahati et al., 2016)
GFP-Modulo	Weischaus Lab (Falahati and Wieschaus, 2017)
Pitchoune-GFP	Weischaus Lab (Falahati and Wieschaus, 2017)
GFP-Rpl135	Weischaus Lab (Blythe et al., 2015)
Su(var)3-906/ TM3Ser	Reuter Lab (Tschiersch et al., 1994)
Su(var)3-917/ TM3Ser	Reuter Lab (Tschiersch et al., 1994)
Mat alpha GAL4	BDSC # 7063
HP1a RNAi	BDSC # 33400
FM6/C(1)DX, y[*] f[1]	BDSC # 784
C(1)RM/C(1;Y)6,y[1]w[1]f[1]/0	BDSC # 9460

Primers

rDNA FISH: 5’-ACGGTTGTTTCGCAAAAGTT-3' and 5’-TGTTGCGAAATGTCTTAGTTTCA-3'

Software and Algorithms

ImageJ (Fiji)	NIH

ZEN Zeiss	Zeiss	https://www.zeiss.com/microscopy/int/products/microscope-software/zen.html
Arivis Vision 4D	Arivis	https://www.arivis.com/
GraphPad Prism	GraphPad	https://www.graphpad.com/

Method Details

Drosophila Stocks and Genetics

All crosses were maintained at 25° C. To visualize the dynamics of HP1a and nucleolar assembly, live embryos from lines *RFP-HP1a; GFP-Fib*, *RFP-Fib; GFP-HP1a* and *RFP-HP1a; GFP-Mod* were imaged. Embryos lacking rDNA were obtained by crossing C(1)DX/Y; *RFP-HP1a; GFP-Fib* or C(1)DX/Y; *RFP-HP1a; Pit-GFP* or C(1)DX/Y; *RFP-Fib; Pit-GFP* virgins to C(1;Y)6,y[1]w[1]f[1]/0 males. 1/4th of the resulting embryos from this cross are predicted to lack rDNA. -rDNA embryos were selected based on the presence of Fibrillarin neocondensates in live and fixed embryos and DAPI morphology in fixed embryos.

To knockdown HP1a in Drosophila embryos, we crossed matα-GAL4 (BDSC #7063) females to HP1a RNAi males (BDSC #33400) to obtain an F1 generation with HP1a depleted in the female germlines. Siblings of the F1 generation were crossed with each other to collect embryos depleted of HP1a. Most of the embryos exhibit severe developmental defects (Park et al., 2019). We selected embryos that reached nuclear cycle 14 for analyses of nucleolar morphology. The study of the effects of HP1a knockdown on the nucleolus was also limited to cycle 14 since most embryos were arrested by this stage.

To analyze nucleolar phenotypes in Su(var)3-9^{null} embryos, we crossed Su(var)3-9^{06} /TM3Ser virgins to Su(var)3-9^{17} /TM3Ser males. After selecting Su(var)3-9$^{06/17}$ adults in the F1 generation, we intercrossed these siblings to collect Su(var)3-9$^{06/17}$ maternal null embryos. However, H3K9me2/3 levels partially recover by the gastrula stage (cycle 15) (through the action of other H3K9me2/3 methyltransferases like Eggless (Seller et al., 2019)), which limited this analysis to cycle 14.

Live Imaging of Drosophila Embryos

To collect Drosophila embryos for live imaging, males and females of the desired genotype were added to a plastic cage covered with apple juice agar plates and left for at least 3 days at 25°C before imaging. On the day of imaging, a fresh plate was added to the cage, and embryos were

collected for two hours. After removing the plate, embryos were coated with Halocarbon oil 27 (Sigma) for staging using a dissection scope with transillumination and then selected for the appropriate stage. Selected embryos were placed on a 2 in x 2 in paper towel square and then dechorionated in 50% bleach for 1 min. Bleach was wicked off with a Kimwipe after 1 min, and then the square was washed with a small amount of distilled water. Excess water was wicked off the square. Dechorionated embryos were secured onto a semipermeable membrane (Lumox film, Starstedt) on a membrane slide holder using Heptane Glue. These embryos were mounted in Halocarbon oil 27 (Sigma) between the membrane and a coverslip. Live imaging was performed on a Zeiss LSM880 Airy Scan microscope (Airy Fast mode) with 63X oil immersion objective at room temperature.

Immunostaining

Embryos were collected on apple juice-agar plates and aged till the appropriate stage. They were dechorionated in 50% bleach and then fixed in 1:1 heptane: 4% formaldehyde in 1XPBS for 25 mins. They were then devitellinized in a 1:1 mixture of methanol: heptane and then stored at -20°C in methanol. Embryos were rehydrated by washing in 1xPBS+0.2% Triton (PBT) and blocked with 2% BSA in PBT. After blocking for ~1hr, embryos were incubated with the primary antibody at 4°C overnight. Following washes with PBT, embryos were incubated with the appropriate secondary antibody at room temperature for 2 hrs, stained in DAPI, and mounted onto a slide using VectaShield (Vector Laboratories) as the mounting medium. All primary antibodies were used at 1:250 dilution and secondaries at 1:1000. Imaging was performed on a Zeiss LSM880 Airy Scan microscope (Airy Fast mode) with 63X oil immersion objective at room temperature.

DNA Fluorescent in situ hybridization (FISH) and combined Immuno-FISH

<u>Probe Labelling</u>

A probe for ITS-1 rDNA was prepared by amplifying an ~800 bp fragment by PCR from genomic DNA using the primers 5'-ACGGTTGTTTCGCAAAAGTT-3' and 5'-TGTTGCGAAATGTCTTAGTTTCA-3'. The PCR product was cloned into a pGEM-Teasy vector (Promega). Using this plasmid as a template, ITS-1 rDNA probe was labelled with Alexa 488, Alexa 555 or Alexa 648 using the FISH Tag™ DNA Multicolor Kit (ThermoFisher) following the manufacturer's protocol. Locked nucleic acid (LNA) oligonucleotides (Integrated DNA technologies) conjugated with Cy5 or FAM were used as probes for 359bp, 1.686 and AAGAG satellite DNA repeats.

Hybridization

Embryos were collected on apple juice-agar plates and aged till the appropriate stage. They were dechorionated in 50% bleach and then fixed in 1:1 heptane: 4% formaldehyde in 1XPBS for 25 mins. They were then devitellinized in a 1:1 mixture of methanol: heptane and then stored in -20°C. Embryos were washed in 2xSSC-T (2xSSC containing 0.1% Tween-20) with increasing formamide concentrations (20%, 40%, then 50%) for 15 min each. 100ng of DNA probes in 40 µl of hybridization solution (50% formamide, 3× SSCT, 10% dextran sulfate) was added, denatured together with the embryos at 95°C for 5 min and incubated overnight at 37°C. Following hybridization, embryos were washed twice in 2xSSCT for 30 mins at 37°C and thrice in PBT for 5 mins at room temperature. After completing washes, embryos were stained in DAPI and mounted onto a slide using VectaShield (Vector Laboratories) as the mounting medium.

Combined Immuno-FISH

For combined in situ detection of proteins and DNA sequences, immunofluorescence was performed first, embryos were post-fixed in 4% formaldehyde for 25mins, and then processed for FISH.

Pan-Protein Staining using 488 NHS Ester

Formaldehyde-fixed embryos were devitellinized in a 1:1 mixture of methanol: heptane and stored in methanol. Embryos were rehydrated by washing in 1xPBS+0.2% Triton (PBT). After washing off methanol, embryos were stained in the diluted 488 NHS ester fluorophore (1:50) from a 10mg/ml stock in 0.1% PBST for 6 h at 4 °C followed by washing in PBT three times for 30 mins each at room temperature. After completing washes, embryos were stained in DAPI for ten minutes and mounted onto a slide using VectaShield (Vector Laboratories) as the mounting medium.

Propidium Iodide Staining

Formaldehyde-fixed and Heptane devitellinized embryos were rehydrated by washing in 1xPBS+0.2% Triton (PBT). Samples were equilibrated in 2X SSC. RNase-treated controls alone were incubated in 100 µg/mL DNase-free RNase in 2X SSC for 20 minutes at 37°C. After washing away the RNase with 2X SSC, embryos were incubated in 500nM of Propidium Iodide in 2X SSC for 10 mins at room temperature. Samples were rinsed in 2X SSC, stained with DAPI, and mounted on a slide with VectaShield (Vector Laboratories) as the mounting medium.

Modeling

To better understand the association of PCH with the nucleolus, we developed a computational model that simulates the interactions between different types of molecules found in these biomolecular condensates. In our computational model, we simulate four components of the nucleus: PCH (H) and ribosomal DNA (rD) as long polymers, and Fibrillarin (F) and an amphiphilic protein (X) as independent, single monomers, which we hereafter refer to as beads. Since the experiments focused on the PCH domain of Drosophila, our computational model only simulates this specific region of the genome (30% of the genome), not the entire genome. This allows us to study the dynamics of this particular region of the genome more accurately and efficiently. PCH is modeled as a semiflexible bead-spring polymer chain in which N beads are connected by N-1 harmonic springs. Each bead of the chain represents a cluster of PCH containing approximately 5 kilo base pairs of DNA, with a diameter of approximately 30 nm. The semi-flexibility of the chain is determined by its persistence length, which is taken to be 60 nm (2 beads) in accordance with previous studies that indicate chromatin has a persistence length between 50 to 100 nm (Wachsmuth et al., 2016). We represent rDNA as a self-avoiding chain that occupies approximately 20% of the middle domain of PCH. Fibrillarin and the amphiphilic protein X are modeled using single, diffusive beads where each protein has distinct interactions with the polymer and other proteins.

To simplify the model, we assume that the size of each protein bead is equal to the size of the heterochromatin bead, with both having a diameter σ. The non-bonding interactions between polymer-polymer, protein-protein, and polymer-protein are modeled using a standard Lennard-Jones (LJ) potential. The LJ potential is truncated at the distance 2.5 σ, meaning that the interaction between the beads is only non-zero if they are within 2.5 σ distance. At very short distances between the beads, the LJ potential is strongly repulsive (representing the excluded volume of two molecules). At intermediate spacings, the LJ potential is attractive, with a strength adjusted to model the different states of chromatin, such as its compaction or decondensation, and the phase-separating tendency of the proteins. In our model, the polymer and the proteins are confined within a spherical boundary that represents the nucleus of the cell. This boundary mimics the effect of the nuclear envelope, which constrains the movement of these beads and affects their interactions with each other. In our study, we used the LAMMPS (Large-scale Atomic/Molecular Massively Parallel Simulator) package to simulate the behavior of our biomolecular system (Thompson et al., 2022). LAMMPS uses Brownian dynamics, which accounts for the viscous forces acting on the beads, and a stochastic force (Langevin thermostat)

to ensure that the system of beads and solvent is maintained at a constant temperature (NVT ensemble). This allows us to accurately model the interactions between the polymer-polymer, polymer-protein, and protein-protein beads and study the behavior of the system over time.

Rationale for the choice of parameters in the coarse-grained model

To analyze the experimental observations of phase separation in the nucleus, we study a minimal model with four crucial components: PCH (H), rDNA (rD), Fibrillarin (F), and an amphiphilic protein (X) that binds both nucleolar and PCH components. The parameters in the simulations include the number of molecules of each component α (N_α), the strength of the attractions between two components (denoted by indices β and γ, $\epsilon_{\beta\gamma}$), and the size of the confinement (R_c). The fraction of the nucleus that is hydrated (does not contain PCH or the other proteins) is obtained from the relative difference between the confinement volume and the volumes of PCH and the other proteins.

<u>Bonding potential between monomers in the polymer made of PCH and rDNA:</u> Adjacent beads on the polymer chain are interconnected by harmonic springs using the potential function:

$$V_s = \sum_{i=1}^{N-1} k_s (r_i - \sigma)^2$$

Here, r_i represents the distance between the i-th and $(i+1)$-th beads. The spring constant and equilibrium distance between neighboring beads are denoted as k_s and σ respectively. In our simulations, the spring constant k_s is set to $100 k_B T/\sigma^2$ to ensure the presence of rigid bonds between adjacent beads of the polymer chain.

<u>Attraction strength</u> ($\epsilon_{\beta\gamma}$): The Lennard-Jones potential is used to model the attraction between any two non-bonded beads:

$$V_{\beta\gamma}(r) = \begin{cases} 4\epsilon_{\beta\gamma}\left[\left(\frac{\sigma}{r}\right)^{12} - \left(\frac{\sigma}{r}\right)^{6}\right] & \text{for } r \le r_c \\ 0 & \text{for } r > r_c \end{cases}$$

Here, the symbol $\epsilon_{\beta\gamma}$ represents the attraction strength between beads of type β and γ, where $\beta, \gamma \in \{H, rD, F, X\}$ represent PCH, rDNA, Fibrillarin, and amphiphilic protein, respectively. For instance, ϵ_{FX} represents the attraction strength between Fibrillarin and amphiphilic protein beads. When dealing with attractive interactions between chromatin-chromatin and chromatin-protein beads, a distance cutoff of $r_c = 2.5\sigma$ is used for the Lennard-Jones potential, beyond which the interaction is set to zero. To account for only excluded volume interactions (with no attractions) using the same potential, a cutoff of $r_c = 2^{1/6}\sigma$ and $\epsilon = 1 k_B T$ are employed. This choice is made

because the potential energy is at its minimum at that point, and the resulting force on a bead is zero. As there are four components in our model, there are a total of 10 combinations ((n(n+1)/2), where n is number of components) of attraction strength parameters between the different components.

Confinement size: The size of the confinement is determined by defining the volume fraction of chromatin ϕ:

$$\phi = N_G \times \frac{\text{volume of 1 bead}}{\text{volume of confinement}} = N_G \times \frac{(\frac{4}{3}\pi\sigma^3)}{(\frac{4}{3}\pi R_c^3)}$$

Here, N_G represents the total number of beads in the Drosophila genome, where each bead corresponds to 5 kilobase pairs (kbps) of DNA. The diameter of a spherical bead, denoted as σ, is taken to be 30 nm (see Bajpai & Safran, 2023 for further explanation). The total length of the diploid Drosophila genome is 360 Mbps, and N_G can be calculated by dividing the Drosophila genome length by the amount of DNA represented by one bead (5 kbps). The volume fraction of chromatin (ϕ) is commonly reported as ~ 0.1 in existing literature (Qi & Zhang, 2021; Tripathi & Menon, 2019). Using the equation above, the calculated radius of the confinement (R_c) is found to be 45σ.

Number of molecules in PCH and rDNA: We model the PCH domain as a polymer chain composed of $N = 10{,}000$ beads, which represents approximately 30% of the beads in the entire genome. Among these $10{,}000$ beads, 20% are designated as rDNA, resulting in a total of $4{,}000$ rDNA beads. We do not explicitly model the rest of the genome since the experiments show that the nucleolar components are localized near PCH.

Concentration of Fibrillarin and amphiphilic protein: The concentration of Fibrillarin and amphiphilic protein is calculated as follows:

$$\text{concentration } (c_\alpha) = \frac{N_\alpha}{\text{volume of confinement}}$$

Here, the symbol α represents the type of protein, where $c_\alpha = c_F$ for the fibrillarin concentration and $c_\alpha = c_X$ for the amphiphilic protein concentration. After defining the parameters and obtaining the value for the confinement radius parameter from the assumed volume fraction of PCH, we proceed with an initial simulation, focusing on a single component, namely the fibrillarin protein, within the confinement. During this simulation, we vary the concentration (c_F) and the attraction strength (ϵ_{FF}) of Fibrillarin. Our experimental results demonstrate that Fibrillarin undergoes phase separation independently of the other components (rDNA or PCH) during cycle 14 (refer to Figure 3A). These initial-stage simulation results yield a phase diagram, which indicates that a minimum

attraction strength of $1.3 - 2.0 k_{\mathrm{B}}\mathrm{T}$ is required to condense fibrillarin particles within the concentration range of $c_F = 0.0013 - 0.013$. The reported concentration of nucleolar particles is $c = 0.015$ (Qi & Zhang, 2021). Consequently, we maintain a fixed concentration of Fibrillarin at $c_F = 0.013$ when simulating all the other protein components. Since the concentration of amphiphilic protein is not determined from the experiments, we conducted multiple simulations, systematically varying the amphiphilic protein concentration (c_X) within the range of $0.0013 - 0.13$. The results of these simulations are discussed in Supplementary Figure 5A.

<u>Parameter range of ϵ_{HH}</u>: To understand the behavior of each component separately (before including interactions between different components) in the next stage, we conducted simulations specifically focusing only on the PCH chain. The PCH chain represents a condensed chromatin region within the nucleus which implies self-attractive interactions of the beads representing the polymer. During these simulations, we varied the attraction strength between PCH beads (ϵ_{HH}) from 0 to $0.5 k_{\mathrm{B}}\mathrm{T}$. Our results revealed that within the range of $\epsilon_{HH} = 0.35 - 0.5\, k_{\mathrm{B}}\mathrm{T}$ (see Supplementary Figure 5D), the PCH chain underwent collapse, resulting in a condensed conformation that is phase-separated from the aqueous component of the system (not simulated explicitly).

<u>Parameter value of ϵ_{rD-F}</u>: We next simulate the self-organization due to the interactions between the three components (where each component so far was considered alone): PCH, rDNA, and Fibrillarin. We set $\epsilon_{HH} = 0.35\, k_{\mathrm{B}}\mathrm{T}$ and $\epsilon_{FF} = 2\, k_{\mathrm{B}}\mathrm{T}$, incorporating only excluded-volume interactions (hard-core, repulsive interactions) between H-F, i.e., there is no direct attraction between PCH and Fibrillarin as implied by the experiments. By varying the attraction strength between rDNA and Fibrillarin (ϵ_{rD-F}), we made the following observations based on our simulation results: a weaker attraction (and $\epsilon_{rD-F} = 0.75\, k_{\mathrm{B}}\mathrm{T}$) resulted in rDNA wrapping around the condensed Fibrillarin phase, while a stronger attraction (and $\epsilon_{rD-F} = 2\, k_{\mathrm{B}}\mathrm{T}$) led to the condensation of rDNA within the Fibrillarin complex. This latter observation aligns with our experimental findings. Therefore, we select $\epsilon_{rDF} = 2\, k_{\mathrm{B}}\mathrm{T}$ as the parameter value in the subsequent simulations.

<u>Parameter ranges of ϵ_{FF} and ϵ_{XX}:</u> Finally, we introduce the fourth component, an amphiphilic protein, which we suggest may interact attractively with both PCH and Fibrillarin. Initially, we investigated the relative attraction strengths between Fibrillarin and amphiphilic protein when considering the same concentration for both. We explore all possible combinations of ϵ_{FF} both greater than and less than ϵ_{XX}. For $\epsilon_{XX} \geq \epsilon_{FF}$, we observe PCH surrounding the amphiphilic protein-rich phase, but just a partial wetting between the amphiphilic protein-rich phase and the Fibrillarin-rich phase (see Supplementary Figure 5C). Only when $\epsilon_{XX}\epsilon_{FF}$, do we observe PCH

surrounding the amphiphilic protein-rich phase, which in turn surrounds the Fibrillarin condensate, consistent with the experiments in the wild type.

Parameter range of ϵ_{FX}: We proceeded to vary the attraction strength between Fibrillarin and amphiphilic proteins within the range of $\epsilon_{FX} = 1.5k_{\mathrm{B}}\mathrm{T}$. When the attraction strength is relatively low ($\epsilon_{FX} \leq 0.75k_{\mathrm{B}}\mathrm{T}$), the fibrillarin-rich phase and the amphiphilic protein-rich phase do not associate with each other. At moderate attraction strengths ($\epsilon_{FX} \geq 1k_{\mathrm{B}}\mathrm{T}$ and ($\epsilon_{FX} \leq 1.25k_{\mathrm{B}}\mathrm{T}$), the Fibrillarin-rich and amphiphilic protein-rich phases partially wet each other. Finally, at higher attraction strengths (($\epsilon_{FX} = 1.5k_{\mathrm{B}}\mathrm{T}$), the amphiphilic protein completely wets Fibrillarin (see Supplementary Figure 5E)).

Parameter range of c_X: Additionally, we explored variations in the concentration of amphiphilic protein (c_X). Notably, for higher concentrations of amphiphilic protein ($c_X = 0.005 - 0.013$), we observed that heterochromatin tends to completely engulf the amphiphilic protein-rich phase, which in turn engulfs Fibrillarin (see Supplementary Figure 5A).

Quantitative Image Analysis

3D measurements were performed using Arivis Vision4D (Zeiss) while ImageJ was used for all 2D measurements. The details of each analysis pipeline used in this study are listed below:

Measuring the fraction of the nucleolar edge occupied by HP1a

Figure 2B: A cluster of nuclei were manually chosen for analyses ~15-30 mins into the specified interphase and defined as “Early Cycle”, while those observed ~50-70 mins were defined as “Late Cycle”. Preprocessing steps include background subtraction and denoising using Gaussian blur. HP1a and Fibrillarin were segmented in 3D using the "Intensity Threshold Segmenter" with the Auto segmentation method. To calculate the fraction of the nucleolar edge occupied by HP1a, the nucleolus was dilated by 1 pixel and subtracted from the dilated object to create a 1-pixel shell around the nucleolus. The nucleolus shell was intersected with HP1a segments to calculate the volume of the nucleolar shell that overlaps with HP1a.

Measuring Distances

Figure 1E and 2D: Preprocessing steps include background subtraction and denoising using Gaussian blur. 1.686 or 359bp foci and Fibrillarin were manually segmented using the "Intensity Threshold Segmenter" with the Simple segmentation method. The distance between a Fibrillarin segment and its nearest 1.686 or 359bp locus was measured in 3D using the "Distances" feature in Arivis.

Figure 3B: HP1a and Fibrillarin were segmented using the "Intensity Threshold Segmenter" with the Auto segmentation method. The distance between HP1a and its nearest Fibrillarin segment was measured in 3D using the "Distances" feature in Arivis.
Figure 3F: AAGAG and 1.686 were segmented using the "Intensity Threshold Segmenter" with the Auto segmentation method. The distance between AAGAG and its nearest 1.686 segment was measured in 3D using the "Distances" feature in Arivis.

Measuring Aspect Ratio of HP1a

Figure 3D: Individual nuclei were manually selected 15 mins after the start of Cycle 15. Preprocessing steps include background subtraction and denoising using Gaussian blur. HP1a was segmented using Auto thresholding using Otsu. The aspect ratio of the segment was determined using the Analyze Particles feature in Fiji.

Line Scans:

Figure 4B: Line scans were generated using the "Plot profile" feature in Fiji. The highest intensity value in the green and magenta channels were each set to 1.0, and the remaining intensities were normalized to it.

Pitchoune void formation measurements

Figure 6E-G: To measure the dynamics of the formation of Pitchoune in -rDNA embryos, maximum intensity projections of Amnioserosa were first preprocessed in Fiji using Subtract background and a Gaussian Blur filter. Auto thresholding for each time point was performed using the Yen method. Using Analyze Particles, the area, circularity and mean intensity of each segment of Pitchoune was extracted. The mean intensity over time was normalized to its value at T=0.

Measuring Volume

Supplementary Figure 3: Preprocessing steps include background subtraction and denoising using Gaussian blur. The volume of segments was extracted using Arivis after Fibrillarin was segmented in 3D using the "Intensity Threshold Segmenter" with the Auto segmentation method (Otsu feature).

Statistical Analysis

Data were plotted, and statistical analyses were performed using GraphPad Prism8. P-values were calculated using unpaired two-tailed t-tests.

ACKNOWLEDGEMENTS

We thank Eric Weischaus (Princeton University) and Shelby Blythe (Northwestern University) for generously sharing the fluorescently tagged nucleolar fly lines. We thank Lucy Brennan, Coral Zhou, and Collin Hickmann for their careful reading and feedback on the manuscript. SS and GHK are grateful for the support of the Volkswagen Foundation.

AUTHOR CONTRIBUTIONS

SR: conceptualization, experimentation, data acquisition, formal analysis, validation, investigation, methodology, and writing

OA: conceptualization, investigation, formal analysis, and writing

GB: simulations, data acquisition, formal analysis, methodology, and writing

KL: experimentation and data acquisition

SC: reagent preparation and formal analysis

SS: writing, and funding acquisition

GHK: conceptualization, writing, and funding acquisition

COMPETING INTERESTS

No competing interests to declare.

REFERENCES

Ahmad, K., & Henikoff, S. (2022). The Drosophila embryo as a tabula rasa for the epigenome. *Faculty Reviews*, *11*(40). https://doi.org/10.12703/R/11-40

Alberti, S., & Hyman, A. A. (2021). Biomolecular condensates at the nexus of cellular stress, protein aggregation disease and ageing. *Nature Reviews Molecular Cell Biology 2021 22:3*, *22*(3), 196–213. https://doi.org/10.1038/s41580-020-00326-6

Bajpai, G., & Safran, S. (2023). Mesoscale, long-time mixing of chromosomes and its connection to polymer dynamics. *PLOS Computational Biology*, *19*(5), e1011142. https://doi.org/10.1371/JOURNAL.PCBI.1011142

Berry, J., Weber, S. C., Vaidya, N., Haataja, M., Brangwynne, C. P., & Weitz, D. A. (2015). RNA transcription modulates phase transition-driven nuclear body assembly. *Proceedings of the National Academy of Sciences of the United States of America*, *112*(38), E5237–E5245.

Bersaglieri, C., Kresoja-Rakic, J., Gupta, S., Bär, D., Kuzyakiv, R., Panatta, M., & Santoro, R. (2022). Genome-wide maps of nucleolus interactions reveal distinct layers of repressive chromatin domains. *Nature Communications 2022 13:1*, *13*(1), 1–18. https://doi.org/10.1038/s41467-022-29146-2

Bizhanova, A., & Kaufman, P. D. (2021). Close to the edge: Heterochromatin at the nucleolar and nuclear peripheries. *Biochimica et Biophysica Acta - Gene Regulatory Mechanisms*, *1864*(1), 194666. https://doi.org/10.1016/j.bbagrm.2020.194666

Bizhanova, A., Yan, A., Yu, J., Zhu, L. J., & Kaufman, P. D. (2020). Distinct features of nucleolus-associated domains in mouse embryonic stem cells. *Chromosoma*, *129*(2), 121–139. https://doi.org/10.1007/S00412-020-00734-9

Brangwynne, C. P., Mitchison, T. J., & Hyman, A. A. (2011). Active liquid-like behavior of nucleoli determines their size and shape in Xenopus laevis oocytes. *Proceedings of the National Academy of Sciences*, *108*(11), 4334–4339. https://doi.org/10.1073/pnas.1017150108

Buchwalter, A., & Hetzer, M. W. (2017). Nucleolar expansion and elevated protein translation in premature aging. *Nature Communications*. https://doi.org/10.1038/s41467-017-00322-z

Dembowski, J. A., Kuo, B., & Woolford, J. L. (2013). Has1 regulates consecutive maturation and processing steps for assembly of 60S ribosomal subunits. *Nucleic Acids Research*, *41*(16), 7889. https://doi.org/10.1093/NAR/GKT545

Dillinger, S., Straub, T., & Németh, A. (2017). Nucleolus association of chromosomal domains is largely maintained in cellular senescence despite massive nuclear reorganisation. *PLOS ONE*, *12*(6), e0178821. https://doi.org/10.1371/journal.pone.0178821

Ditlev, J. A., Case, L. B., & Rosen, M. K. (2018). Who's In and Who's Out—Compositional Control of Biomolecular Condensates. *Journal of Molecular Biology*, *430*(23), 4666–4684. https://doi.org/10.1016/j.jmb.2018.08.003

Eissenberg, J. C., & Elgin, S. C. (2000). The HP1 protein family: getting a grip on chromatin. *Current Opinion in Genetics & Development*, *10*(2), 204–210. https://doi.org/10.1016/S0959-437X(00)00058-7

Falahati, H., Pelham-Webb, B., Blythe, S., & Wieschaus, E. (2016). Nucleation by rRNA dictates the precision of nucleolus assembly. *Current Biology*, *26*(3), 277–285. https://doi.org/10.1016/j.cub.2015.11.065

Falahati, H., & Wieschaus, E. (2017). Independent active and thermodynamic processes govern the nucleolus assembly in vivo. *Proceedings of the National Academy of Sciences*, *114*(6), 1335–1340. https://doi.org/10.1073/pnas.1615395114

Fare, C. M., Villani, A., Drake, L. E., & Shorter, J. (2021). Higher-order organization of biomolecular condensates. *Open Biology*, *11*(6), 210137. https://doi.org/10.1098/rsob.210137

Farrell, J. A., & O'Farrell, P. H. (2014). From Egg to Gastrula: How the Cell Cycle Is Remodeled During the Drosophila Mid-Blastula Transition. *Annual Review of Genetics*, *48*(1), 269–294. https://doi.org/10.1146/annurev-genet-111212-133531

Fefelova, E. A., Pleshakova, I. M., Mikhaleva, E. A., Pirogov, S. A., Poltorachenko, V. A., Abramov, Y. A., Romashin, D. D., Shatskikh, A. S., Blokh, R. S., Gvozdev, V. A., & Klenov, M. S. (2022). Impaired function of rDNA transcription initiation machinery leads to

derepression of ribosomal genes with insertions of R2 retrotransposon. *Nucleic Acids Research*, *50*(2), 867–884. https://doi.org/10.1093/NAR/GKAB1276

Feric, M., Vaidya, N., Harmon, T. S., Mitrea, D. M., Zhu, L., Richardson, T. M., Kriwacki, R. W., Pappu, R. V., & Brangwynne, C. P. (2016). Coexisting Liquid Phases Underlie Nucleolar Subcompartments. *Cell*, *165*(7), 1686–1697. https://doi.org/10.1016/j.cell.2016.04.047

Holmberg Olausson, K., Nistér, M., & Lindström, M. S. (2014). Loss of nucleolar histone chaperone NPM1 triggers rearrangement of heterochromatin and synergizes with a deficiency in DNA methyltransferase DNMT3A to drive ribosomal DNA transcription. *Journal of Biological Chemistry*, *289*(50), 34601–34619. https://doi.org/10.1074/jbc.M114.569244

Janssen, A., Colmenares, S. U., & Karpen, G. H. (2018). Heterochromatin: Guardian of the Genome. *Annual Review of Cell and Developmental Biology*, *34*(1), 265–288. https://doi.org/10.1146/annurev-cellbio-100617-062653

Keenen, M. M., Brown, D., Brennan, L. D., Renger, R., Khoo, H., Carlson, R., Huang, B., Grill, S. W., Narlikar, G. J., & Redding, S. (2020). *HP1 proteins compact DNA into mechanically and positionally stable phase separated domains*. 1–30.

Kelley, F. M., Favetta, B., Regy, R. M., Mittal, J., & Schuster, B. S. (2021). Amphiphilic proteins coassemble into multiphasic condensates and act as biomolecular surfactants. *Proceedings of the National Academy of Sciences of the United States of America*, *118*(51), e2109967118.

Lacy, M. E., & Hutson, M. S. (2016). Amnioserosa development and function in Drosophila embryogenesis: Critical mechanical roles for an extraembryonic tissue. *Developmental Dynamics*, *245*(5), 558–568. https://doi.org/10.1002/DVDY.24395

Lafontaine, D. L. J., Riback, J. A., Bascetin, R., & Brangwynne, C. P. (2020). The nucleolus as a multiphase liquid condensate. *Nature Reviews Molecular Cell Biology*, *22*(3), 165–182. https://doi.org/10.1038/s41580-020-0272-6

Larson, A. G., Elnatan, D., Keenen, M. M., Trnka, M. J., Johnston, J. B., Burlingame, A. L., Agard, D. A., Redding, S., & Narlikar, G. J. (2017). Liquid droplet formation by HP1α suggests a role for phase separation in heterochromatin. *Nature*, *547*(7662), 236–240. https://doi.org/10.1038/nature22822

Larson, K., Yan, S. J., Tsurumi, A., Liu, J., Zhou, J., Gaur, K., Guo, D., Eickbush, T. H., & Li, W. X. (2012). Heterochromatin formation promotes longevity and represses ribosomal RNA synthesis. *PLoS Genetics*. https://doi.org/10.1371/journal.pgen.1002473

Lieberman-Aiden, E., Van Berkum, N. L., Williams, L., Imakaev, M., Ragoczy, T., Telling, A., Amit, I., Lajoie, B. R., Sabo, P. J., Dorschner, M. O., Sandstrom, R., Bernstein, B., Bender, M. A., Groudine, M., Gnirke, A., Stamatoyannopoulos, J., Mirny, L. A., Lander, E. S., & Dekker, J. (2009). Comprehensive mapping of long-range interactions reveals folding principles of the human genome. *Science (New York, N.Y.)*, *326*(5950), 289–293. https://doi.org/10.1126/SCIENCE.1181369

Lyon, A. S., Peeples, W. B., & Rosen, M. K. (2021). A framework for understanding functions of biomolecular condensates on molecular to cellular scales. *Nature Reviews. Molecular Cell Biology*, *22*(3), 215. https://doi.org/10.1038/S41580-020-00303-Z

M'Saad, O., & Bewersdorf, J. (2020). Light microscopy of proteins in their ultrastructural context. *Nature Communications 2020 11:1*, *11*(1), 1–15. https://doi.org/10.1038/s41467-020-17523-8

Németh, A., Conesa, A., Santoyo-Lopez, J., Medina, I., Montaner, D., Péterfia, B., Solovei, I., Cremer, T., Dopazo, J., & Längst, G. (2010). Initial Genomics of the Human Nucleolus. *PLOS Genetics*, *6*(3), e1000889. https://doi.org/10.1371/JOURNAL.PGEN.1000889

Németh, A., & Längst, G. (2011). Genome organization in and around the nucleolus. *Trends in Genetics*, *27*(4), 149–156. https://doi.org/10.1016/j.tig.2011.01.002

Overwijn, D., & Hondele, M. (2023). DEAD-box ATPases as regulators of biomolecular condensates and membrane-less organelles. *Trends in Biochemical Sciences*, *48*(3), 244–258. https://doi.org/10.1016/J.TIBS.2022.10.001

Padeken, J., & Heun, P. (2014). Nucleolus and nuclear periphery: Velcro for heterochromatin. *Current Opinion in Cell Biology*, *28*(1), 54–60. https://doi.org/10.1016/j.ceb.2014.03.001

Padeken, J., Mendiburo, M. J., Chlamydas, S., Schwarz, H.-J., Kremmer, E., & Heun, P. (2013). The Nucleoplasmin Homolog NLP Mediates Centromere Clustering and Anchoring to the Nucleolus. *Molecular Cell*, *50*(2), 236–249. https://doi.org/10.1016/j.molcel.2013.03.002

Park, A. R., Liu, N., Neuenkirchen, N., Guo, Q., & Lin, H. (2019). The Role of Maternal HP1a in Early Drosophila Embryogenesis via Regulation of Maternal Transcript Production. *Genetics*, *211*(1), 201. https://doi.org/10.1534/GENETICS.118.301704

Pederson, T. (2011). The nucleolus. *Cold Spring Harbor Perspectives in Biology*, *3*(3), 1–16. https://doi.org/10.1101/cshperspect.a000638

Politz, J. C. R., Scalzo, D., & Groudine, M. (2013). Something Silent This Way Forms: The Functional Organization of the Repressive Nuclear Compartment. *Annual Review of Cell and Developmental Biology*, *29*(1), 241–270. https://doi.org/10.1146/annurev-cellbio-101512-122317

Pontvianne, F., Blevins, T., Chandrasekhara, C., Mozgová, I., Hassel, C., Pontes, O. M. F., Tucker, S., Mokroš, P., Muchová, V., Fajkus, J., & Pikaard, C. S. (2013). Subnuclear partitioning of rRNA genes between the nucleolus and nucleoplasm reflects alternative epiallelic states. *Genes and Development*, *27*(14), 1545–1550. https://doi.org/10.1101/gad.221648.113

Potapova, T. A., & Gerton, J. L. (2019). *Ribosomal DNA and the nucleolus in the context of genome organization*. 109–127.

Quinodoz, S. A., Ollikainen, N., Tabak, B., Palla, A., Schmidt, J. M., Detmar, E., Lai, M. M., Shishkin, A. A., Bhat, P., Takei, Y., Trinh, V., Aznauryan, E., Russell, P., Cheng, C., Jovanovic, M., Chow, A., Cai, L., McDonel, P., Garber, M., & Guttman, M. (2018). Higher-Order Inter-chromosomal Hubs Shape 3D Genome Organization in the Nucleus. *Cell*, *174*(3), 744-757.e24. https://doi.org/10.1016/j.cell.2018.05.024

Riback, J. A., Zhu, L., Ferrolino, M. C., Tolbert, M., Mitrea, D. M., Sanders, D. W., Wei, M. T., Kriwacki, R. W., & Brangwynne, C. P. (2020). Composition-dependent thermodynamics of intracellular phase separation. *Nature 2020 581:7807*, *581*(7807), 209–214. https://doi.org/10.1038/s41586-020-2256-2

Santoro, R., Li, J., & Grummt, I. (2002). The nucleolar remodeling complex NoRC mediates heterochromatin formation and silencing of ribosomal gene transcription. *Nature Genetics 2002 32:3*, *32*(3), 393–396. https://doi.org/10.1038/ng1010

Schotta, G., Ebert, A., Krauss, V., Fischer, A., Hoffmann, J., Rea, S., Jenuwein, T., Dorn, R., & Reuter, G. (2002). Central role of Drosophila SU(VAR)3-9 in histone H3-K9 methylation and heterochromatic gene silencing. *The EMBO Journal*, *21*(5), 1121–1131. https://doi.org/10.1093/EMBOJ/21.5.1121

Seller, C. A., Cho, C. Y., O'Farrell, P. H., Armstrong, R. L., Duronio, R. J., Seller, C. A., Cho, C. Y., & O'Farrell, P. H. (2019). Rapid embryonic cell cycles defer the establishment of heterochromatin by eggless/SetDB1 in Drosophila. *Genes and Development*, *33*(7–8), 403–417. https://doi.org/10.1101/gad.321646.118

Shin, Y., & Brangwynne, C. P. (2017). Liquid phase condensation in cell physiology and disease. *Science*, *357*(6357), eaaf4382. https://doi.org/10.1126/science.aaf4382

Srivastava, R., Srivastava, R., & Ahn, S. H. (2016). The Epigenetic Pathways to Ribosomal DNA Silencing. *Microbiology and Molecular Biology Reviews : MMBR*, *80*(3), 545. https://doi.org/10.1128/MMBR.00005-16

Strom, A. R., Emelyanov, A. V., Mir, M., Fyodorov, D. V., Darzacq, X., & Karpen, G. H. (2017). Phase separation drives heterochromatin domain formation. *Nature*, *547*(7662), 241–245. https://doi.org/10.1038/nature22989

Thiru, A., Nietlispach, D., Mott, H. R., Okuwaki, M., Lyon, D., Nielsen, P. R., Hirshberg, M., Verreault, A., Murzina, N. V., & Laue, E. D. (2004). Structural basis of HP1/PXVXL motif peptide interactions and HP1 localisation to heterochromatin. *The EMBO Journal*, *23*(3), 489. https://doi.org/10.1038/SJ.EMBOJ.7600088

Thiry, M., & Lafontaine, D. L. J. (2005). Birth of a nucleolus: The evolution of nucleolar compartments. *Trends in Cell Biology*, *15*(4), 194–199. https://doi.org/10.1016/j.tcb.2005.02.007

Thompson, A. P., Aktulga, H. M., Berger, R., Bolintineanu, D. S., Brown, W. M., Crozier, P. S., in 't Veld, P. J., Kohlmeyer, A., Moore, S. G., Nguyen, T. D., Shan, R., Stevens, M. J., Tranchida, J., Trott, C., & Plimpton, S. J. (2022). LAMMPS - a flexible simulation tool for particle-based materials modeling at the atomic, meso, and continuum scales. *Computer Physics Communications*, *271*, 108171. https://doi.org/10.1016/J.CPC.2021.108171

Tortora, M. M. C., Brennan, L. D., Karpen, G., & Jost, D. (2023). HP1-driven phase separation recapitulates the thermodynamics and kinetics of heterochromatin condensate formation. *BioRxiv*, 2022.07.11.499635. https://doi.org/10.1101/2022.07.11.499635

Torza, S., & Mason, S. G. (1969). Coalescence of Two Immiscible Liquid Drops. *Science*, *163*(3869), 813–814. https://doi.org/10.1126/SCIENCE.163.3869.813

Van Koningsbruggen, S., Gierliński, M., Schofield, P., Martin, D., Barton, G. J., Ariyurek, Y., Den Dunnen, J. T., & Lamond, A. I. (2010). High-Resolution Whole-Genome Sequencing Reveals That Specific Chromatin Domains from Most Human Chromosomes Associate with Nucleoli. *Molecular Biology of the Cell*, *21*(21), 3735. https://doi.org/10.1091/MBC.E10-06-0508

van Steensel, B., & Belmont, A. S. (2017). Lamina-associated domains: links with chromosome architecture, heterochromatin and gene repression. *Cell*, *169*(5), 780. https://doi.org/10.1016/J.CELL.2017.04.022

Vertii, A., Ou, J., Yu, J., Yan, A., Pagès, H., Liu, H., Zhu, L. J., & Kaufman, P. D. (2019). *Two contrasting classes of nucleolus-associated domains in mouse fibroblast heterochromatin*. https://doi.org/10.1101/gr.247072.118

Wachsmuth, M., Knoch, T. A., & Rippe, K. (2016). Dynamic properties of independent chromatin domains measured by correlation spectroscopy in living cells. *Epigenetics and Chromatin*, *9*(1), 1–20. https://doi.org/10.1186/S13072-016-0093-1/TABLES/2

Wang, L., Gao, Y., Zheng, X., Liu, C., Dong, S., Li, R., Zhang, G., Wei, Y., Qu, H., Li, Y., Allis, C. D., Li, G., Li, H., & Li, P. (2019). Histone Modifications Regulate Chromatin Compartmentalization by Contributing to a Phase Separation Mechanism. *Molecular Cell*, 1–14. https://doi.org/10.1016/j.molcel.2019.08.019

Zaffran, S., Chartier, A., Gallant, P., Astier, M., Arquier, N., Doherty, D., Gratecos, D., & Séméria, M. (1998). A Drosophila RNA helicase gene, pitchoune, is required for cell growth and proliferation and is a potential target of d-Myc. *Development (Cambridge, England)*, *125*(18), 3571–3584. https://doi.org/10.1242/DEV.125.18.3571

Zhang, H., Wu, Z., Lu, J. Y., Huang, B., Zhou, H., Xie, W., Wang, J., & Shen, X. (2020). DEAD-Box Helicase 18 Counteracts PRC2 to Safeguard Ribosomal DNA in Pluripotency Regulation. *Cell Reports*, *30*(1), 81-97.e7. https://doi.org/10.1016/J.CELREP.2019.12.021

LEGENDS FOR SUPPLEMENTARY MOVIES

Supplementary Movie 1: Live imaging of RFP-Fib (green) and GFP-HP1a (magenta) in nuclear cycle 13.

Supplementary Movie 2: Live imaging of RFP-Fib (green) and GFP-HP1a (magenta) in nuclear cycle 14.

Supplementary Movie 3: Live imaging of RFP-Fib (green) and GFP-HP1a (magenta) in nuclear cycle 15.

Supplementary Movie 4: Live imaging of RFP-Fib (green) and GFP-HP1a (magenta) in nuclear cycle 16.

Supplementary Movie 5: Live imaging of RFP-Fib (green) and GFP-HP1a (magenta) in nuclear cycle 17.

Supplementary Movie 6: Live imaging of GFP-Fib (green) and RFP-HP1a (magenta) in nuclear amnioserosa nuclei in embryos lacking rDNA.

Supplementary Movie 7: Simulations of coarse-grained modeling of rDNA (red), Fibrillarin (green), PCH (magenta), and an amphiphilic protein (yellow) with the parameters listed in the 4X4 matrix in Figure 5B.

Supplementary Movie 8: Live imaging of Pitchoune-GFP (green) and RFP-HP1a (magenta) in nuclear amnioserosa nuclei in embryos lacking rDNA.

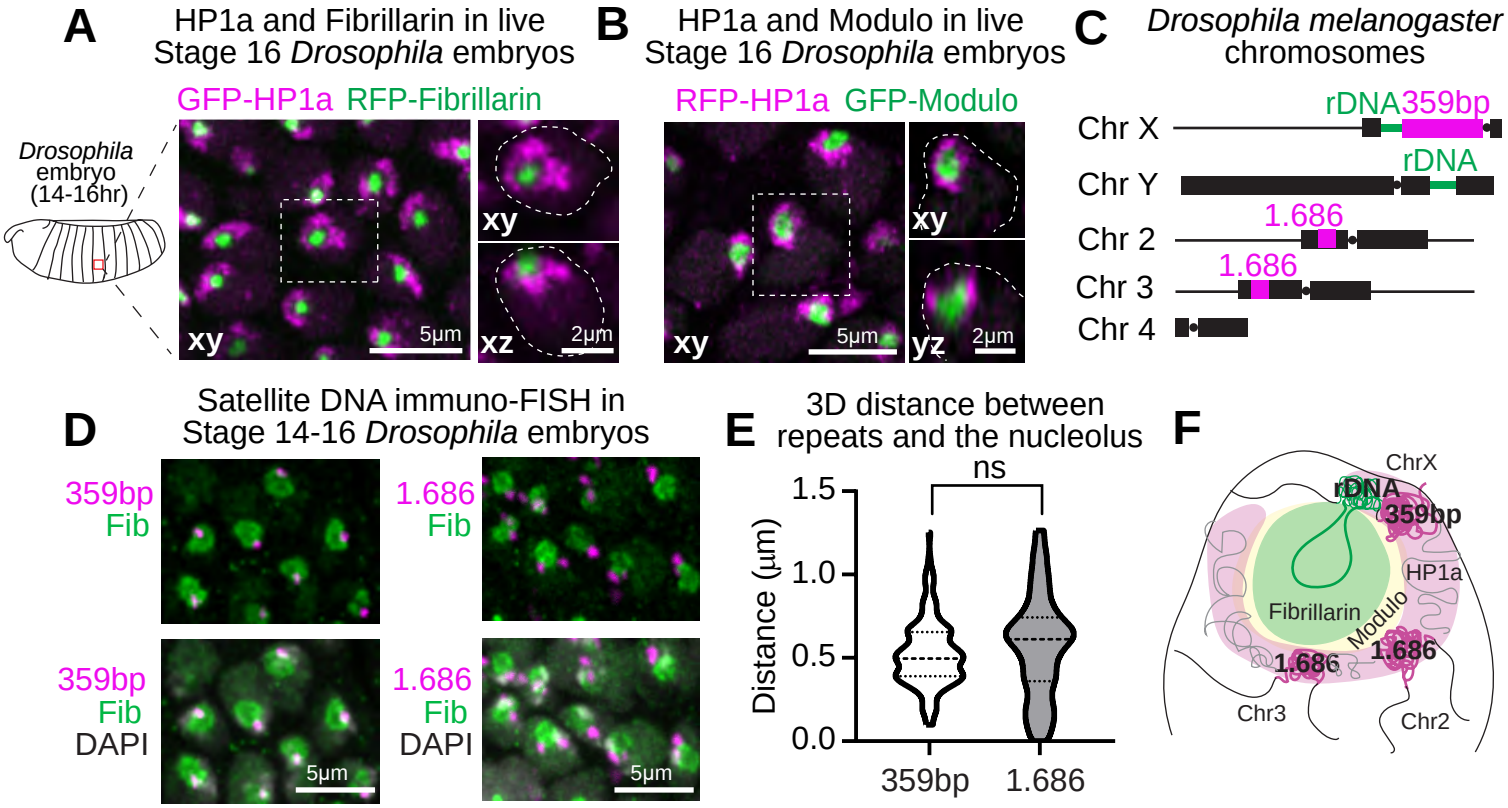

Figure 1: Pericentromeric Heterochromatin (PCH) localizes to the edge of the nucleolus in late *Drosophila* embryos

(A) Representative maximum intensity projections of PCH (GFP-HP1a, magenta) and nucleoli (RFP-Fibrillarin, green) in live epidermal nuclei in a late *Drosophila* embryo (Stage 16, ~14-16hr). The nucleus within the white dashed box is magnified on the right and presented in xy and xz view. White dashed lines indicate the nuclear boundary.

(B) Representative maximum intensity projections of PCH (RFP-HP1a, magenta) and nucleoli (GFP-Modulo, green) in live epidermal nuclei in a late *Drosophila* embryo (Stage 16, ~14-16hr). The nucleus within the white dashed box is magnified on the right and presented in xy and xz view. White dashed lines indicate the nuclear boundary.

(C) Schematic of the locations of pericentromeric satellite repeats (359bp and 1.686) and rDNA repeats in *Drosophila melanogaster* chromsomes.

(D) Combined immuno-FISH (maximum intensity projections) of Fibrillarin (Fib, green) and 359bp (left panel, magenta) or 1.686 (rightpanel, magenta) in nuclei from a late (Stage 14-16) *Drosophila* embryo. Nuclei are co-stained with DAPI (grey).

(E) 3D distances between the centers of geometry of the nucleolus (Fibrillarin) and its nearest 359bp and 1.686 locus in epidermal nuclei of late (Stage 14-16) *Drosophila* embryo. n>125 nuclei (totaled from 3 embryos). ns: not significant.

(F) Schematic of the organization of the nucleolus and PCH in nuclei in late *Drosophila* embryos.

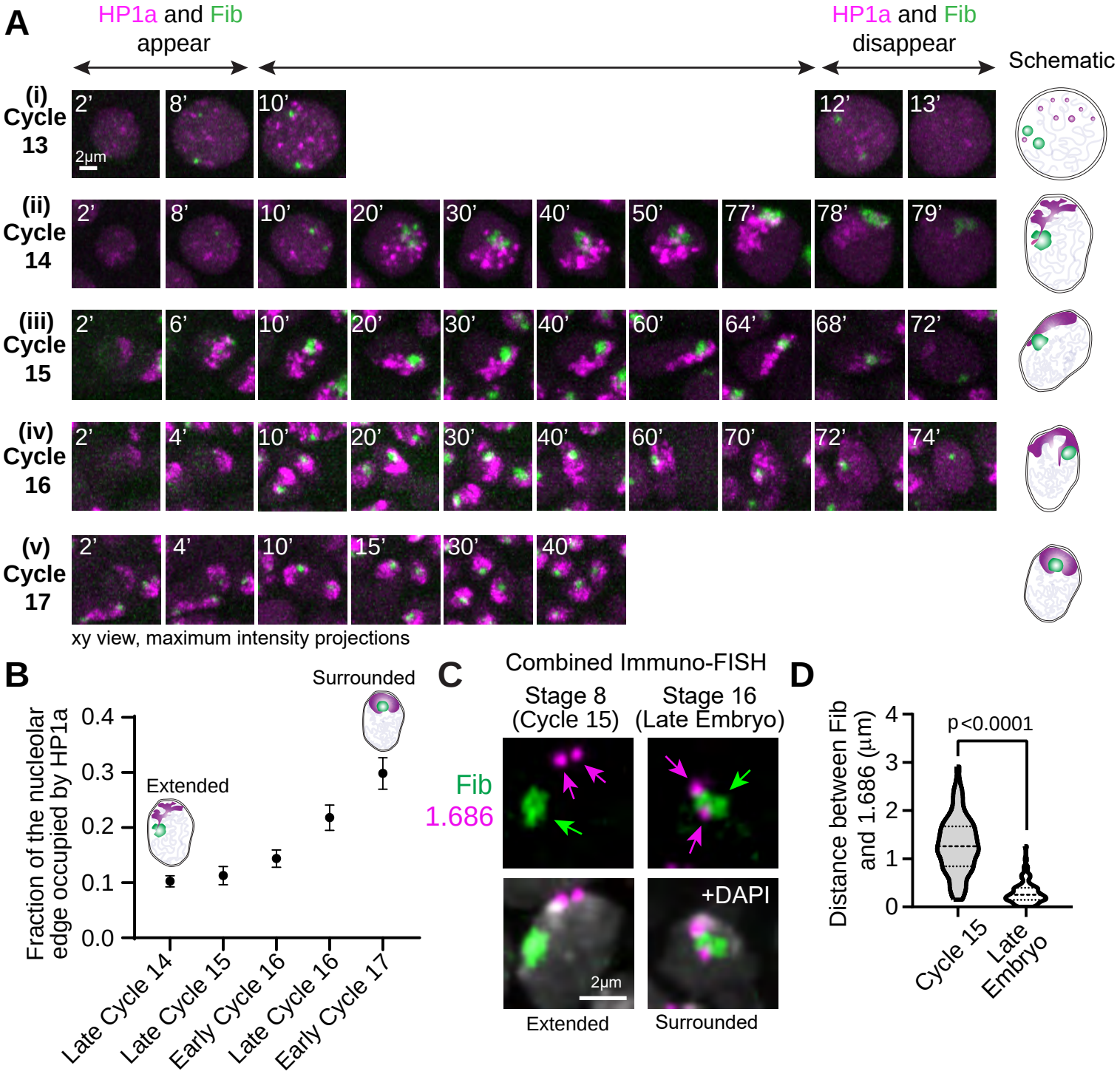

Figure 2: PCH reorganizes from the nuclear to the nucleolar edge during early Drosophila development

(A) Maximum intensity projections (xy view) of individual live nuclei of GFP-HP1a (magenta) and RFP-Fibrillarin (green) in Cycle 13-17 of *Drosophila* embryogenesis. The numbers on the top left corner of each image indicate the time passed after mitotic exit.

(B) Quantification of the fraction of the nucleolar edge occupied by HP1a at specific developmental cycles. "Early Cycle" refers to nuclei observed between 15-30 mins, while "Late Cycle" refers to nuclei observed between 50-70 mins into the specified interphase. The data points represent the mean and the error bars represent the 95% confidence intervals around the mean. n>50 nuclei at each time point (totaled from 5 embryos).

(C) Combined immuno-FISH of 1.686 (magenta arrows), Fibrillarin (green arrow) and DAPI (grey) in a nucleus from epidermal cells of Stage 8 (~Cycle 15) and Stage 16 (Late) *Drosophila* embryos.

(D) Distance between the centers of geometry of 1.686 and Fibrillarin in Stage 8 (~Cycle 15) and Stage 16 (Late) in *Drosophila* nuclei. n>60 loci (totaled from 3 embryos) at each developmental stage.

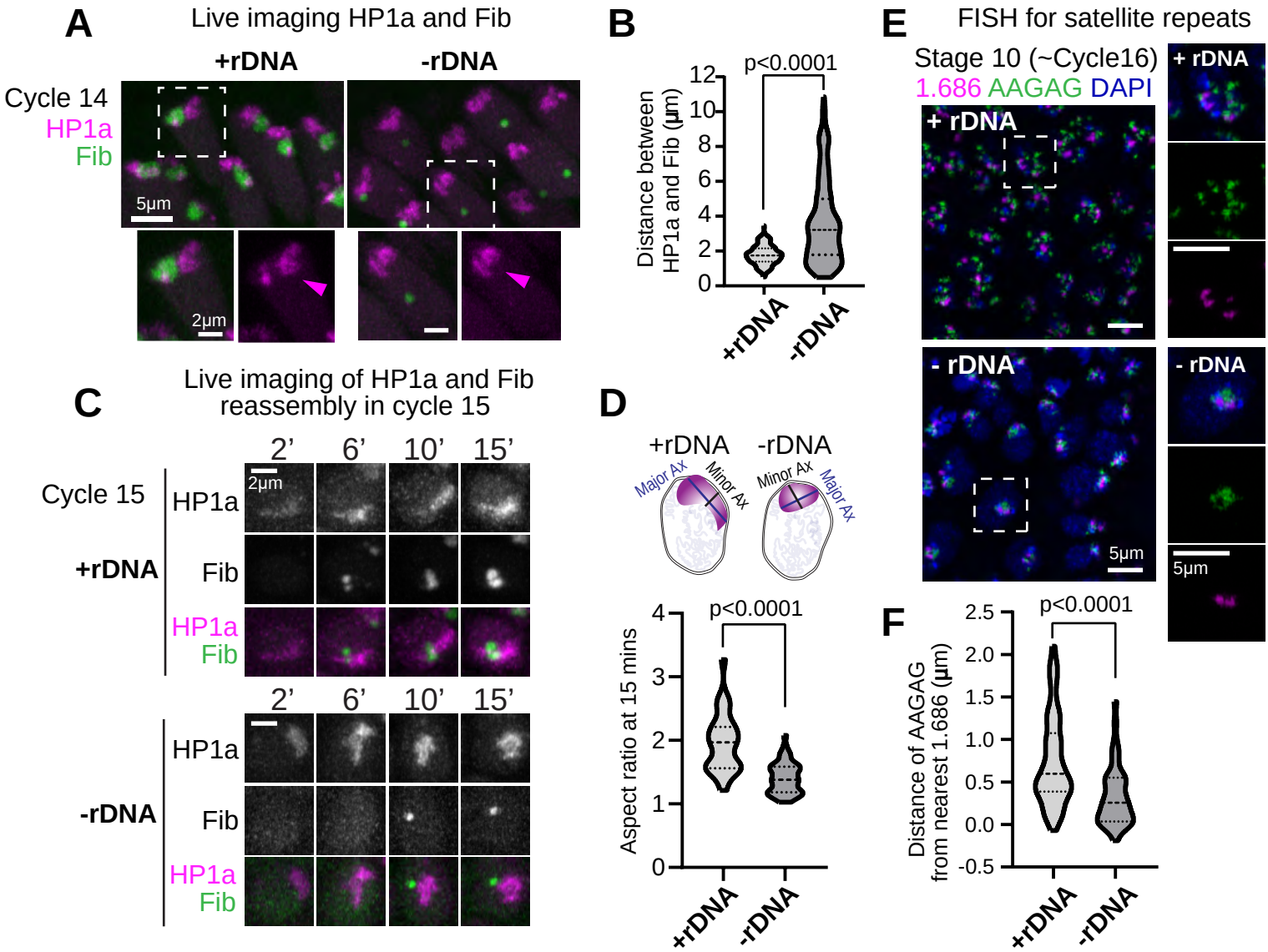

Figure 3: Increased PCH compaction in embryos lacking rDNA

(A) Maximum intensity projections of live nuclei from wildtype embryos (+rDNA) and mutant embryos lacking rDNA (-rDNA) at Cycle 14 showing RFP-HP1a (magenta) and GFP-Fibrillarin (green). The dashed box highlights the nuclei enlarged in the panel below.

(B) Distance between the centers of geometry of HP1a and Fibrillarin in +rDNA and -rDNA embryos. n>200 nuclei (totalled from 5 embryos) in each genotype.

(C) Maximum intensity projections from live imaging of nuclei from +rDNA and -rDNA embryos showing the reassembly of RFP-HP1a (magenta) and GFP-Fibrillarin (green) at the indicated minutes after the start of Cycle 15.

(D) Quantification of the aspect ratio (major axis over minor axis) of HP1a segments 15 minutes after the start of Cycle 15 in +rDNA and -rDNA embryos. n>30 nuclei in each genotype.

(E) Maximum intensity projections of FISH (Fluorescence In Situ Hybridization) of 1.686 (magenta) and AAGAG (green) in DAPI (blue)-stained nuclei in +rDNA and -rDNA Stage 10 embryos. The dashed boxes mark the nuclei enlarged on the right.

(F) Quantification of the distance between AAGAG and its nearest 1.686 locus. n>40 pairs of loci in each genotype.

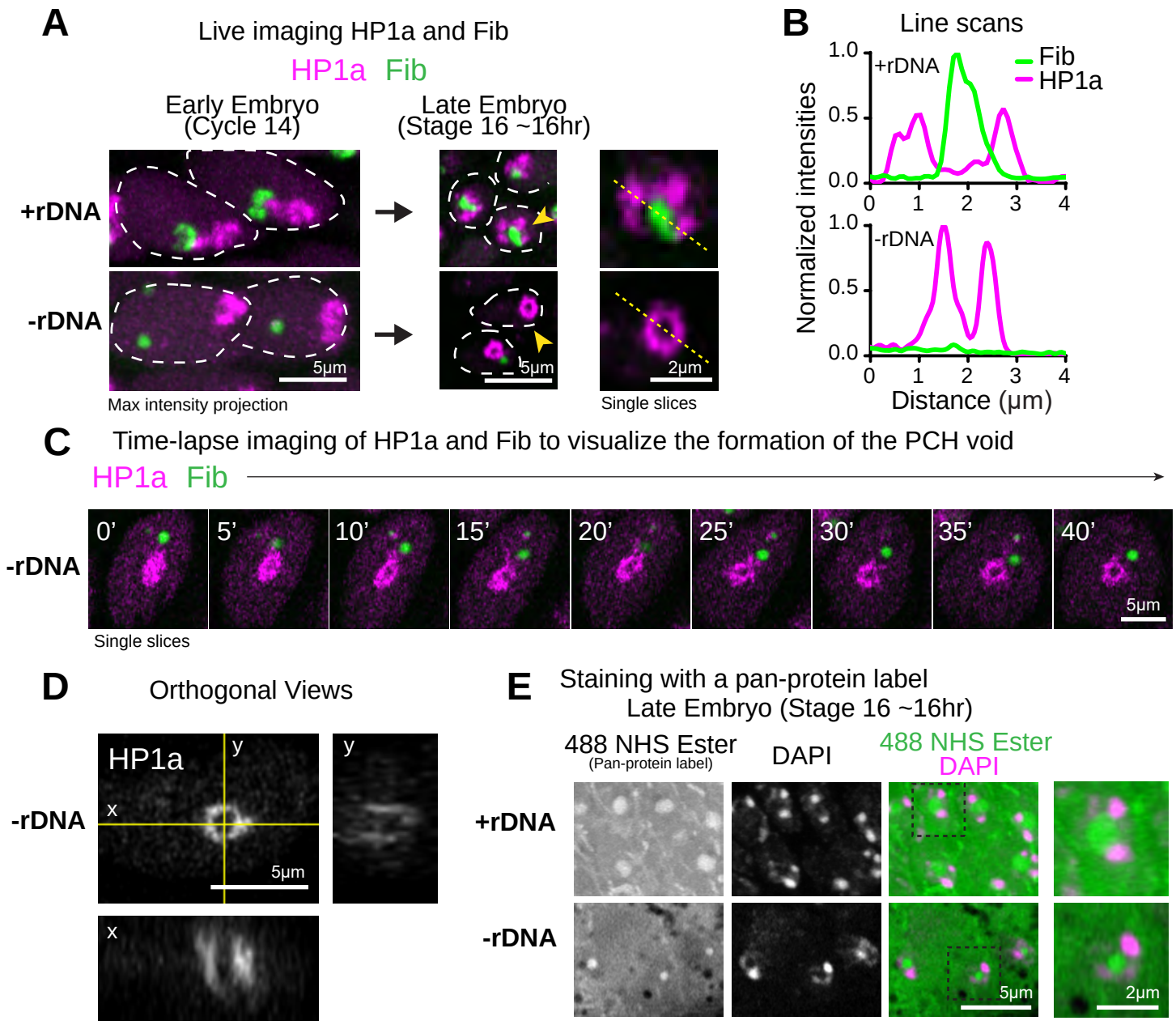

Figure 4: A protein-filled core reshapes the PCH condensate to a hollow sphere-like structure in -rDNA developing embryos

(A) Representative stills of live +rDNA and -rDNA nuclei at Cycle 14 and in Stage 16 (late stage) embryos showing RFP-HP1a (magenta) and GFP-Fibrillarin (green). Nuclei marked with the yellow arrowhead are enlarged on the right.

(B) Line scans of the intensity of the dashed yellow line in the optical slices in (A)

(C) Time-lapse stills (single slices) of a -rDNA amnioserosa nucleus with RFP-HP1a (magenta) and GFP-Fibrillarin (green).

(D) Orthogonal views (single slices) of RFP-HP1a in a -rDNA live amnioserosa nucleus. The yellow lines indicate the location of the orthogonal slices.

(E) Late embryos (Stage 16) with the +rDNA or -rDNA genotype were co-stained with a pan-protein label, 488 NHS Ester (green) and DAPI (magenta). Nuclei marked with the black dashed box are enlarged on the right.

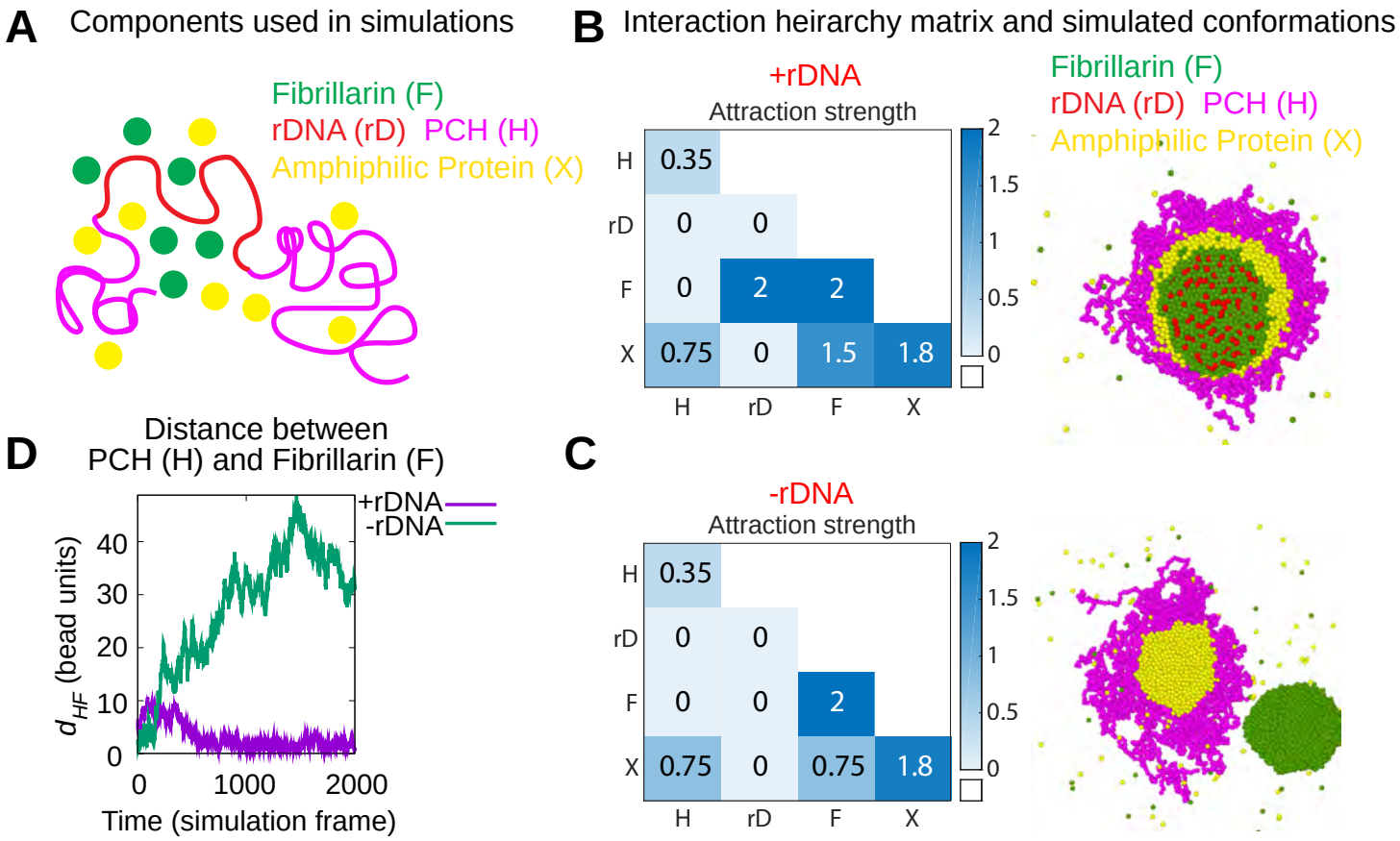

Figure 5: A heirarchy of interaction strengths between PCH, nucleoli and 'amphiphilic' protein(s) recapitulates in vivo +rDNA and -rDNA phenotypes.

(A) Course-grained modelling of nucleolar-PCH assembly with four minimal components: PCH (H) as a self-interacting polymer, rDNA (rD) as polymeric block embedded within PCH, Fibrillarin (F) as a representative of a self-associating nucleolar protein, and an 'amphiphilic' protein (X) that has an affinity for both PCH and nucleolar components.

(B and C) Interaction matrix indicates the strength of interaction (units: k_BT) between Fibrillarin (F), rDNA (rD), PCH (H) and an unknown amphiphilic protein (X) and simulated outcome in +rDNA and -rDNA, with simulated outcomes on the right.

(**D**) Distance (d_{HF}) between the centers of mass of the PCH (H) and Fibrillarin (F) in +rDNA and -rDNA simulations.

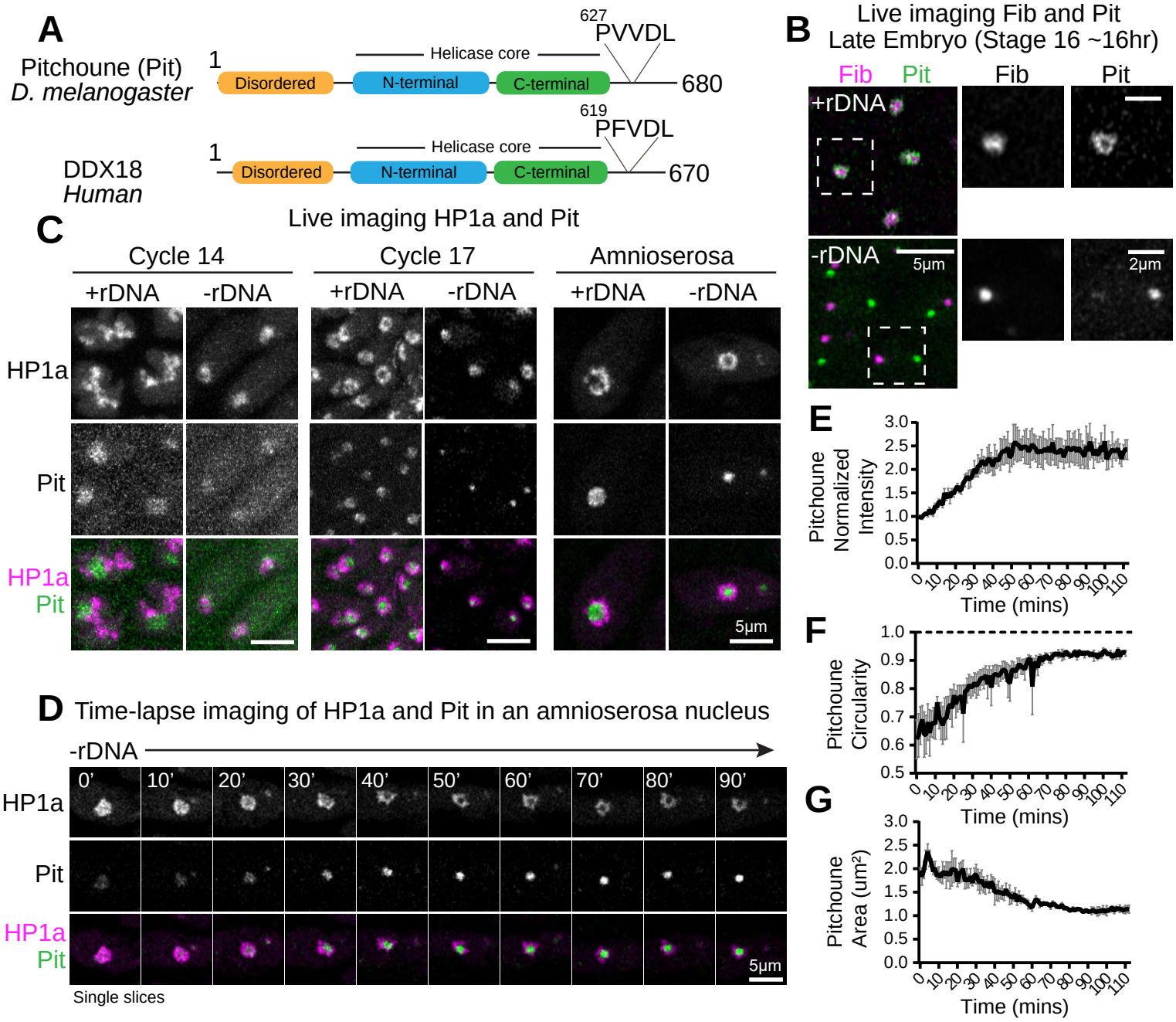

Figure 6: The DEAD-Box RNA Helicase Pitchoune is enriched in the PCH void in -rDNA embryos
(A) Protein subdomains including a conserved PXVXL domain in Pitchoune (Pit) and its human ortholog DDX18.
(B) Representative images of epidermal nuclei from late stage Drosophila embryos with +rDNA and -rDNA genetic backgrounds with RFP-Fibrillarin (magenta) and Pitchoune-GFP (green). Nuclei marked with the white dashed box are enlarged on the right.
(C) Maximum intensity projections of Cycle 14, Cycle 17 and amnioserosa nuclei from +rDNA and -rDNA embryos showing RFP-HP1a (magenta) and Pitchoune-GFP (green).
(D) Time-lapse stills (single slices) of a -rDNA amnioserosa nuclei with RFP-HP1a (magenta) and Pitchoune-GFP (green).
(E) Mean intensity, **(F)** Circularity, and **(G)** Area of projections of Pitchoune increases in -rDNA embryos. Mean of 35-60 nuclei at each time point in n= 3 embryos. Error Bars: SEM.

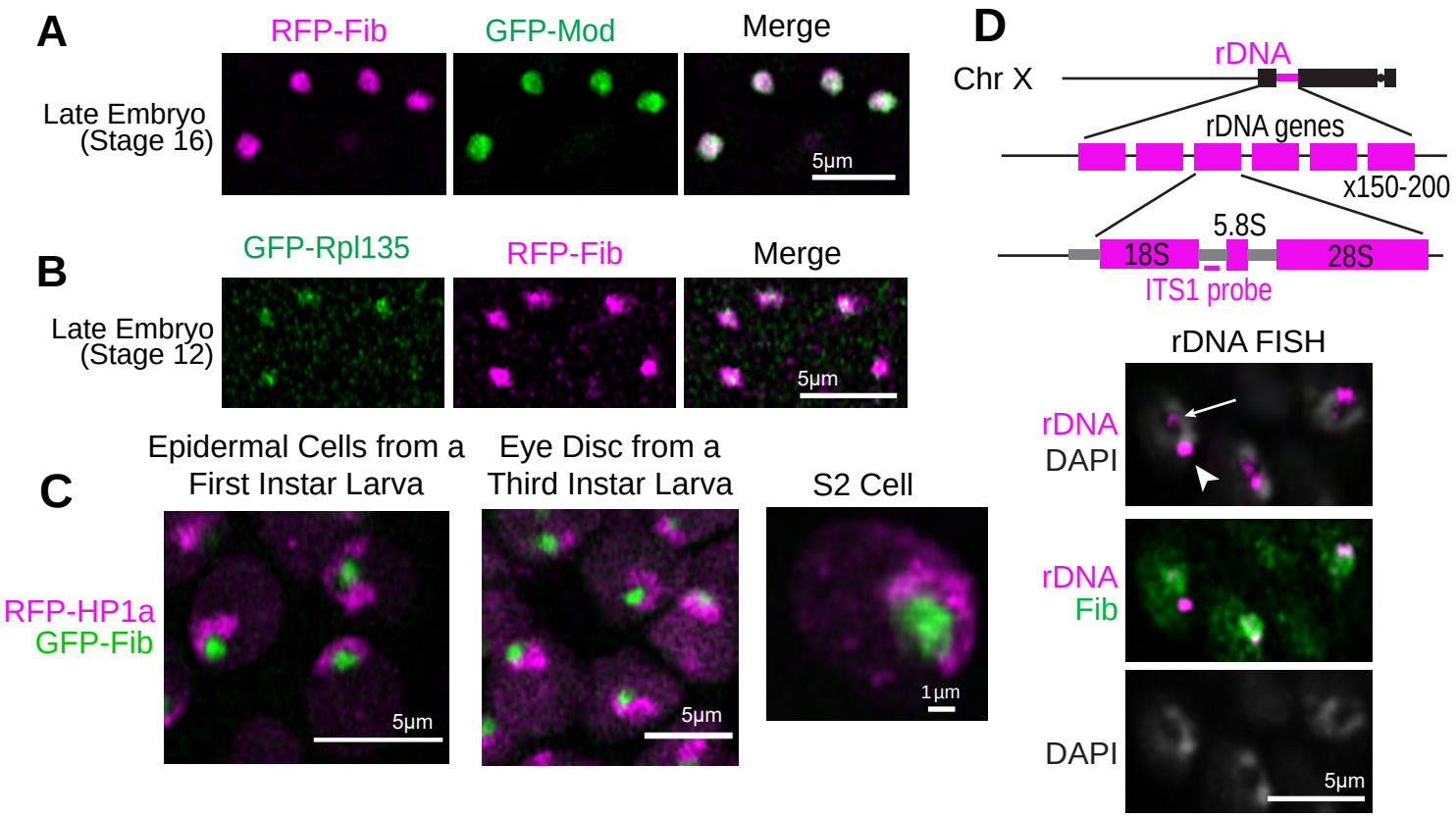

Supplementary Figure 1: The nucleolus is surrounded by PCH in Drosophila nuclei
(**A**) Representative images of nucleoli indicating the distribution of GFP-Modulo (green) and RFP-Fib (magenta) in a live late (Stage 16) embryo.
(**B**) Representative images of nucleoli indicating the distribution of GFP-Rpl135 (green) and RFP-Fib (magenta) in a live late (Stage 12) embryo.
(C) Representative stills of nuclei from epidermal cells from first instar larvae (left), eye disc from third instar larvae (center), S2 cell culture (right). Magenta, RFP-HP1a. Green, GFP-Fibrillarin.
(D) Top: Schematic of ribosomal DNA (rDNA) array in *Drosophila melanogaster* showing the position of the ITS-1 rDNA probe. Bottom: Combined immuno-FISH in fixed late embryos with the ITS-1 rDNA probe (magenta), Fibrillarin (green) and DAPI (gray). The high-intensity rDNA signal (white arrow-head) is located at the edge of the nucleolus while a low intensity rDNA signal (white arrow) is observed inside the nucleolus.

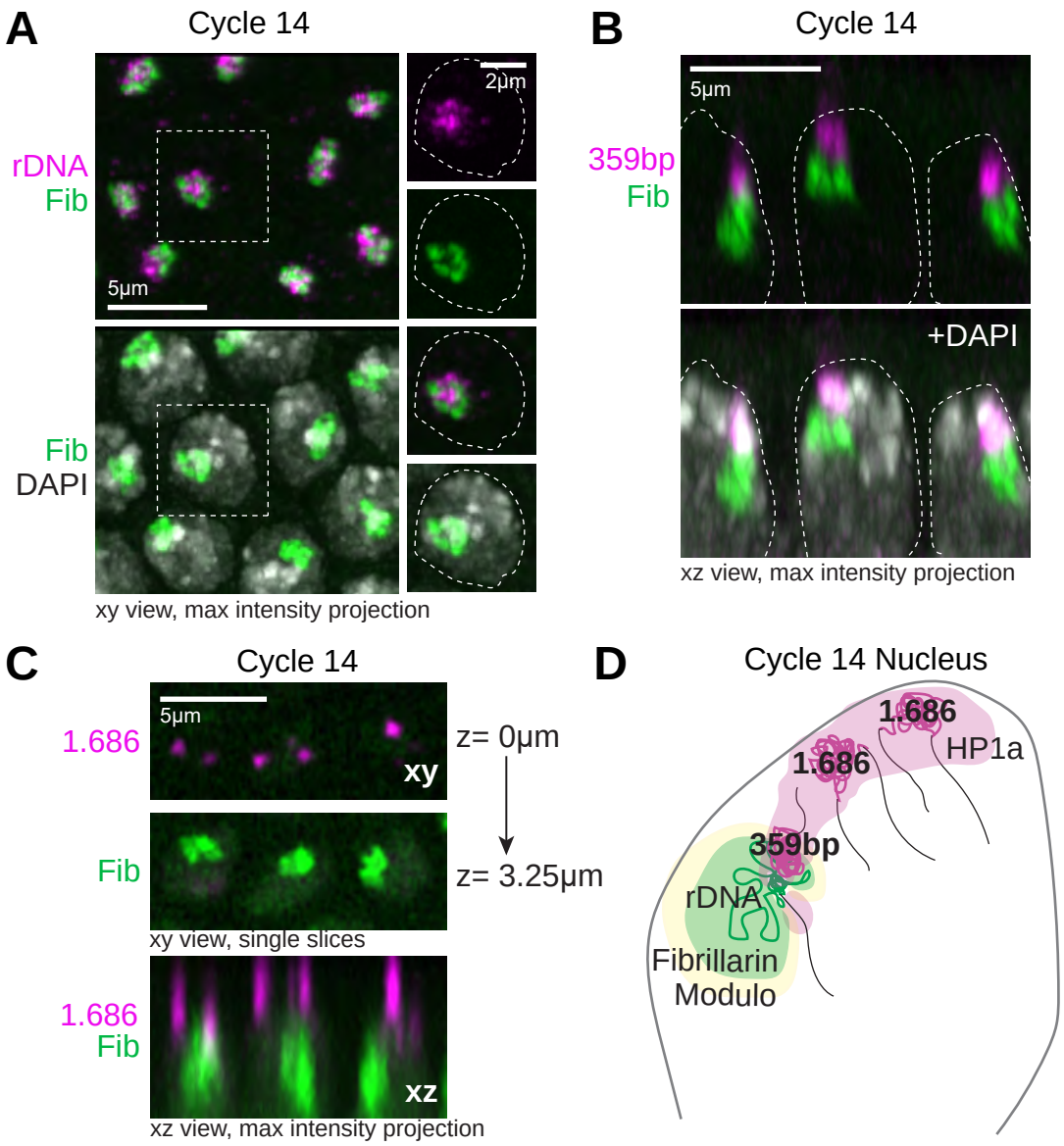

Supplementary Figure 2: Distribution of rDNA and pericentromeric satellite repeats in Cycle 14
Combined immuno-FISH of Drosophila nuclei in Cycle 14 stained for Fibrillarin (green), DAPI (gray) and **(A)** ITS-1 rDNA (magenta), **(B)** 359bp satellite DNA (magenta) on Chr X and **(C)** 1.686 satellite DNA (magenta) on Chr 2 and 3. Dashed white lines represent the edge of the nucleus determined by DAPI staining.
D) Schematic of the distribution of satellite repeats on the X, 2 and 3 chromosomes in Drosophila nuclei in Cycle 14.

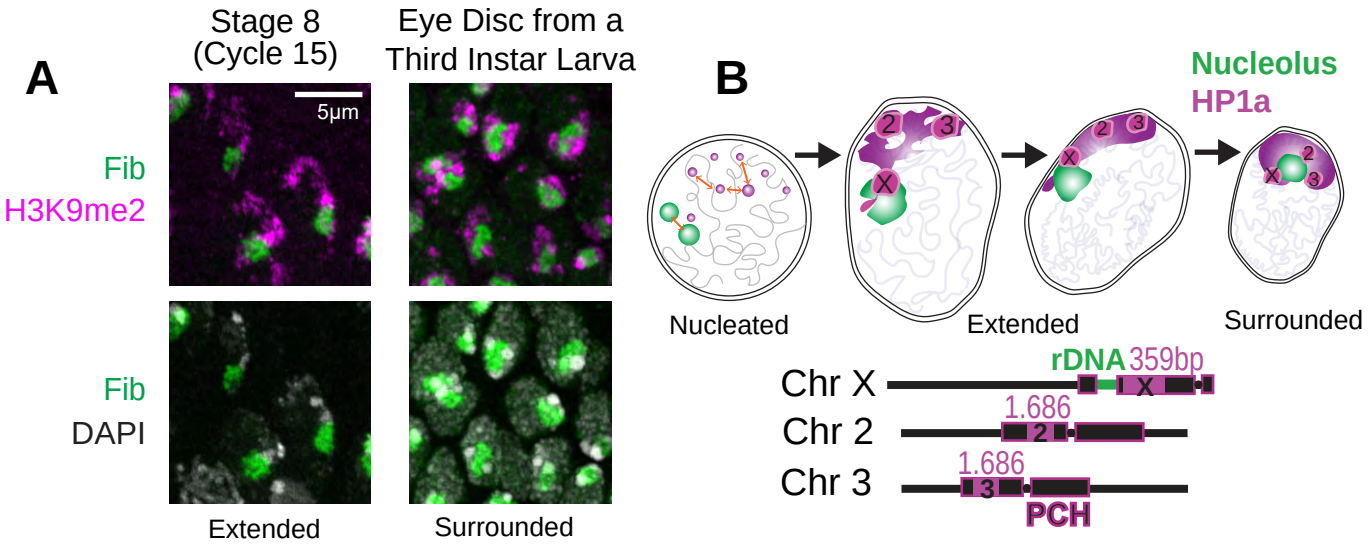

Supplementary Figure 3: PCH is reorganized around the nucleolus during Drosophila development

(A) Immunofluorescence of H3K9me2 (magenta), Fibrillarin (green) and DAPI (gray) in nuclei from a Stage 8 (~Cycle 15) and eye disc from a third instar larva.

(B) Model illustrating the reorganization of PCH around the nucleolus during Drosophila development. Initially, PCH (magenta) and nucleolar (green) condensates are spatially separated, nucleating independently. Subsequently, through growth and fusion events (indicated by orange arrows), the majority of PCH becomes associated with the nuclear edge while remaining tethered at one end of the nucleolus, resulting in an "extended" organization. As the embryo develops, PCH repeats (represented by numbered magenta circles) and HP1a progressively reorganize around the nucleolus, ultimately forming a "surrounded" organization.

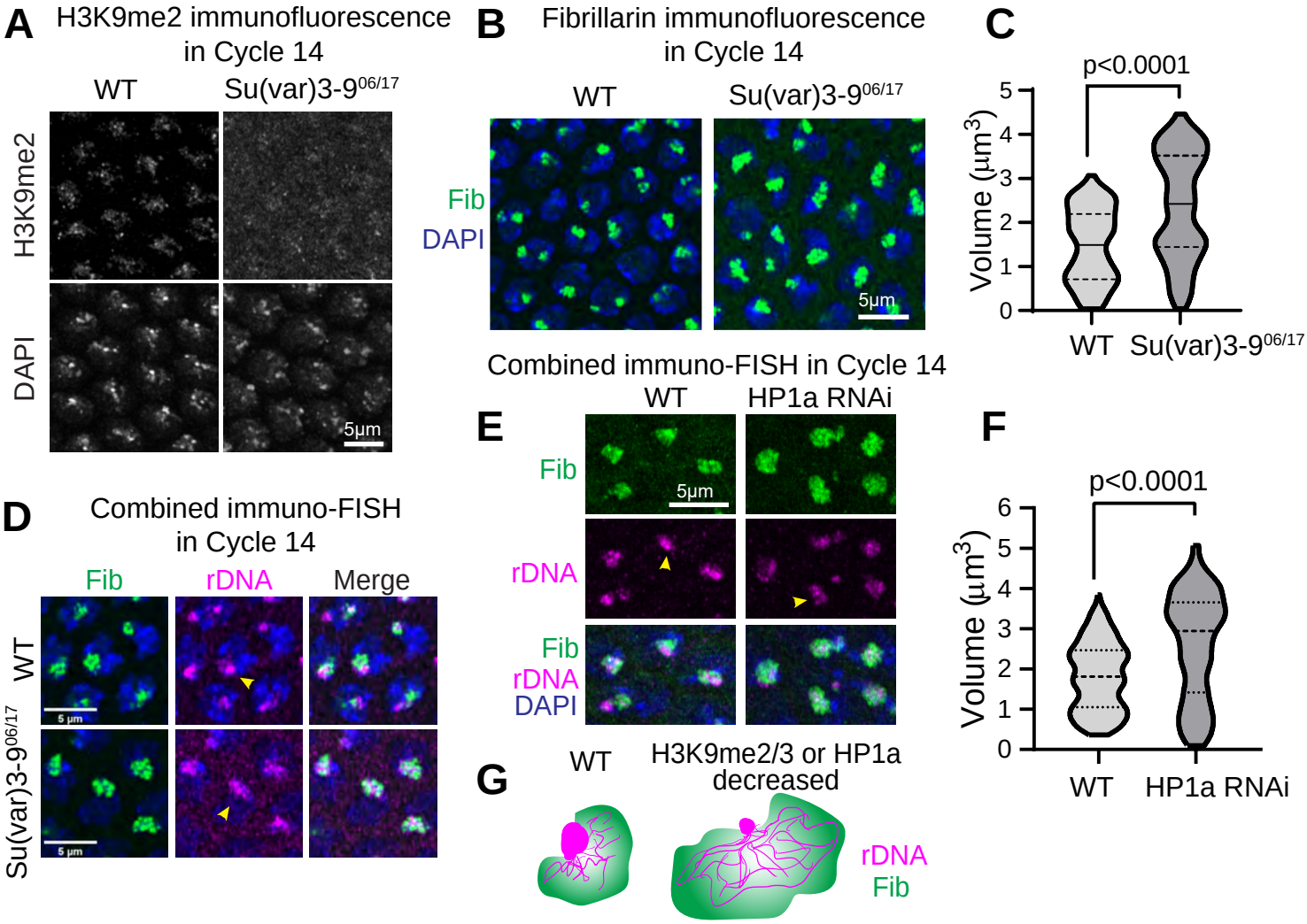

Supplementary Figure 4: The nucleolus is enlarged, and rDNA is decondensed when H3K9 methylation or HP1a is reduced

(A) Maximum intensity z projections of WT and Su(var)3-9$^{06/17}$ nuclei immunostained with H3K9me2 (green) and co-stained with DAPI (blue) at nuclear cycle 14.

(B) Maximum intensity z projections of nuclei immunostained with Fibrillarin (green) and costained with DAPI (blue) in WT and Su(var)3-9$^{06/17}$ embryos at Cycle 14.

(C) Quantification of the volume of Fibrillarin in WT and Su(var)3-9$^{06/17}$ embryos at Cycle 14.

(D) Combined immuno FISH (maximum intensity z projections) of Fibrillarin (green), rDNA (magenta) and DAPI (blue) in WT and Su(var)3-9$^{06/17}$ embryos at Cycle 14.

(E) Maximum intensity z projections of nuclei from wildtype and HP1a RNAi embryos at Cycle 14. Fibrillarin (green), rDNA (red), DAPI (blue)

(F) Volume of Fibrillarin in WT and HP1a RNAi in embryos at Cycle 14.

(G) Schematic of the observed phenotypes depicting decondensation of rDNA and nucleolar enlargement when H3K9me2/3 or HP1a is decreased.

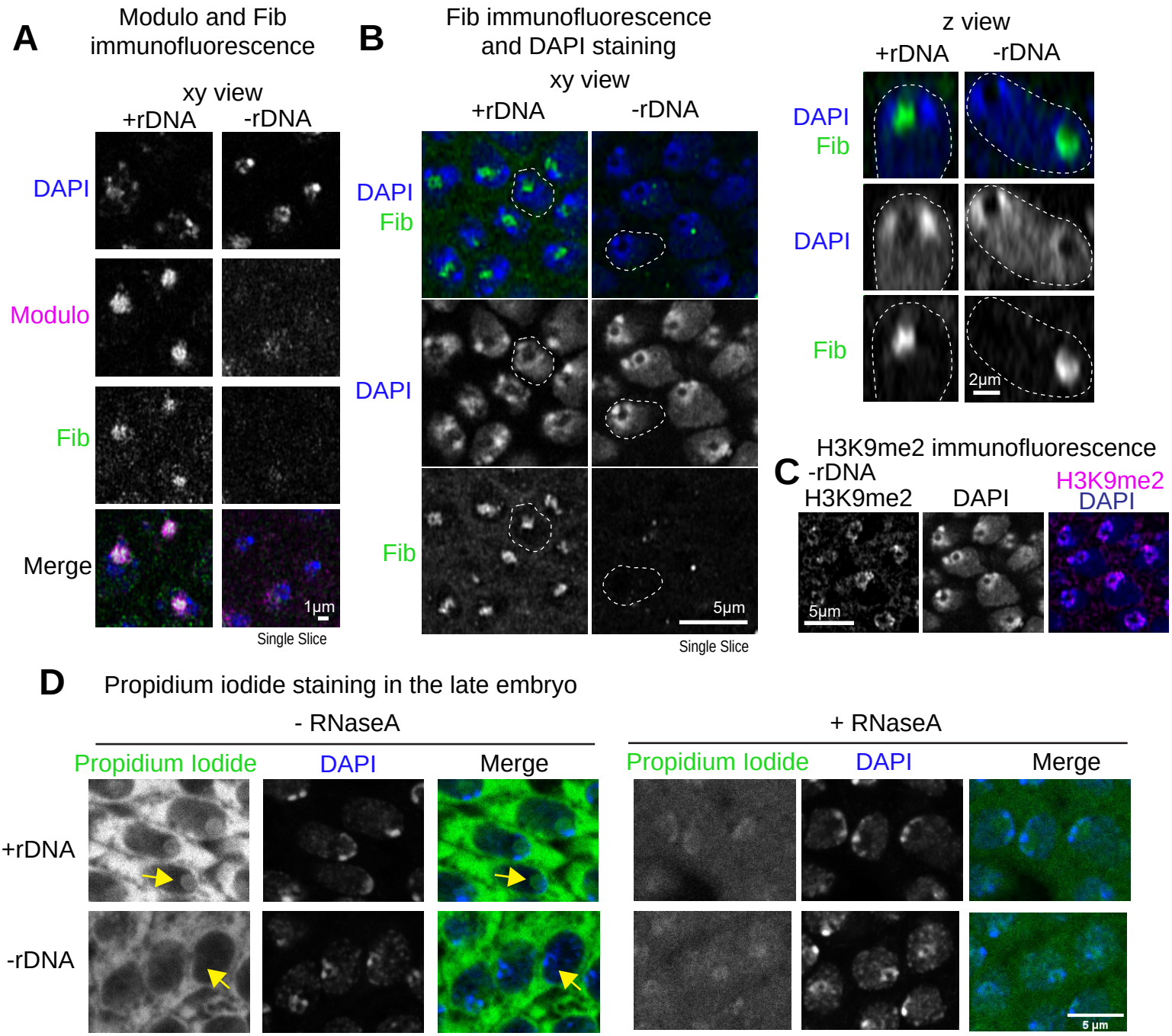

Supplementary Figure 5: The HP1a-void in -rDNA embryos does not stain for DAPI, Fibrillarin, Modulo or Propidium Iodide (RNA)

(A) Representative images of fixed nuclei from wildtype late embryos and mutant embryos lacking rDNA stained for Modulo (magenta), Fibrillarin (green) and DAPI (blue).

(B) Left: Representative images of fixed nuclei from Stage 14-16 (late) wildtype embryos and mutant embryos lacking rDNA showing Fibrillarin (green) and DAPI (blue). Right: Nuclei marked with white dashed outlines on the left are shown in the z plane.

(C) H3K9me2 immunofluorescence (magenta) and DAPI (blue) staining in -rDNA nuclei in Stage 14-16 (late) Drosophila embryos.

(D) Representative images of fixed nuclei from Stage 14-16 (late) wildtype and mutant embryos lacking rDNA stained with Propidium Iodide (green) and DAPI (blue) without (left) and with (right) RNaseA. The yellow arrow points to the RNA staining in the the nucleolus in +rDNA and lack of propodium iodide staining in -rDNA nuclei.

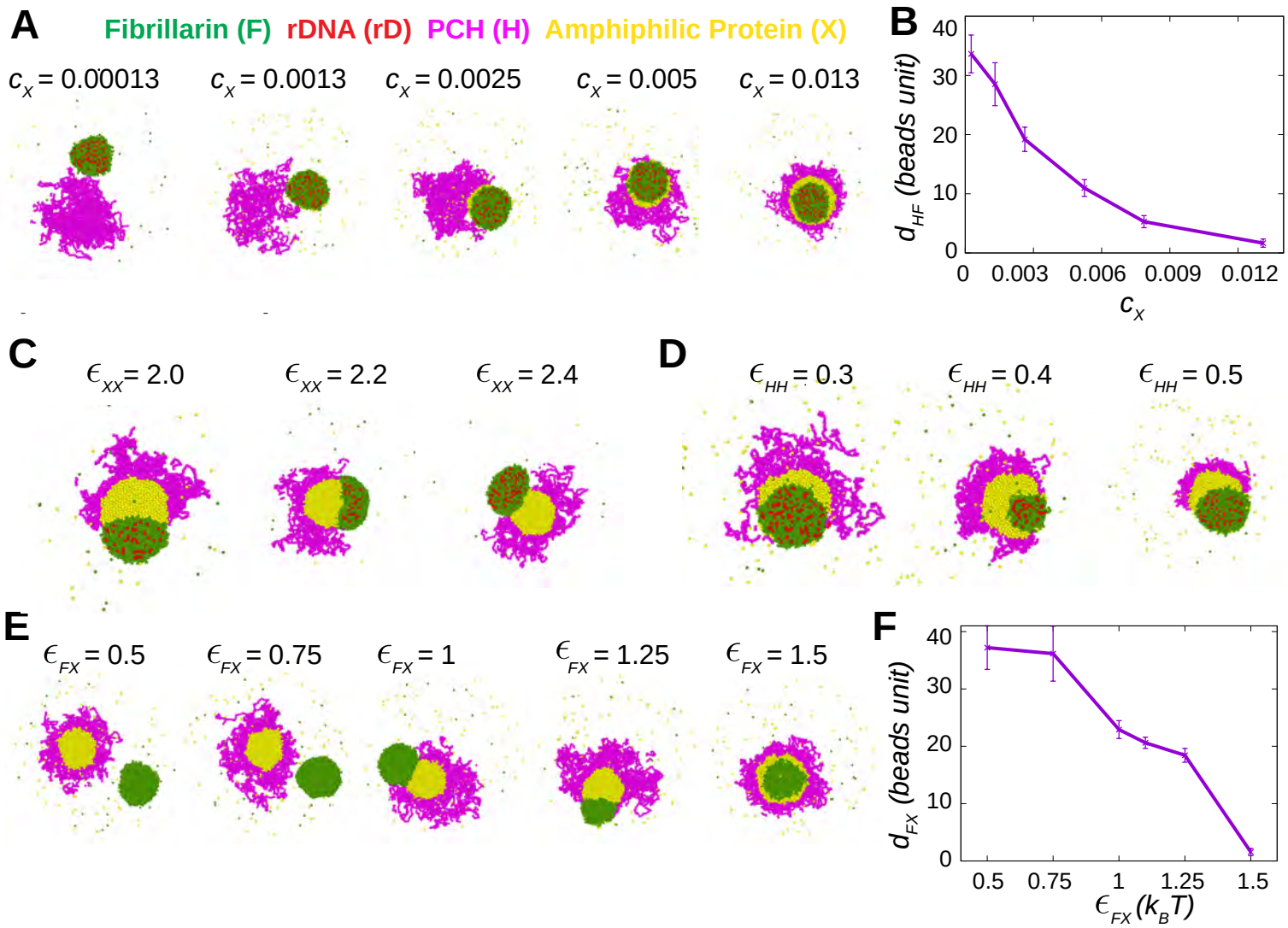

Supplementary Figure 6: Coarse-grained model for the assembly of the nucleolus and PCH
(**A**) Simulation endpoint snapshots demonstrate how increasing the concentration (c_X) of an amphiphilic protein X (yellow), facilitates the association of PCH (H) (magenta) around the Fibrillarin condensate (F) (green).
(**B**) The average distance (d_{HF}) between the PCH (H) and Fibrillarin (F) clusters from their center of mass is measured for different protein X concentrations (c_X). Error Bars represent standard deviation (SD).
(**C**) Simulation endpoint snapshots depict the outcomes of varying X-X attraction strengths (ϵ_{XX}).
(**D**) Simulation endpoint snapshots depict the outcomes of varying the attraction strengths between beads of the PCH (H) polymer chain (ϵ_{HH}) .
(**E**) Simulation endpoint snapshots depict the outcomes of varying attraction strengths between Fibrillarin and protein X (ϵ_{FX}) in the -rDNA condition.
(**F**) The average distance (d_{FX}) between Fibrillarin and protein X condensates from their center of mass is measured for different attraction strengths. Error Bars represent SD.